

A Stochastic Mobility-Driven Spatially Explicit SEIQRD COVID-19 Model with VOCs, Seasonality, and Vaccines

Tijs W. Alleman^{1,2*†}, Michiel Rollier^{1*†}, Jenna Vergeynst^{1,2}
and Jan M. Baetens¹

¹KERMIT, Department of Data Analysis and Mathematical Modelling, Ghent University, Coupure Links 653, Ghent, 9000, Belgium.

²BIOMATH, Department of Data Analysis and Mathematical Modelling, Ghent University, Coupure Links 653, Ghent, 9000, Belgium.

*Corresponding author(s). E-mail(s): tijs.alleman@ugent.be;
michiel.rollier@ugent.be;

†These authors contributed equally to this work.

Abstract

Key message: We add spatial heterogeneity and interprovincial mobility, variants of concern, seasonality, and vaccination, to a previously established epidemiological model. We simulate the model stochastically using the Tau-leaping method. We demonstrate its ability to describe past COVID-19 incidence, to generate projections for policymakers and to study the influence of mobility on SARS-CoV-2 spread. We assess if adding the impact of spatial heterogeneity and interprovincial mobility is worth the added complexity.

Abstract: In this work we extend our previously developed compartmental SEIQRD model for SARS-CoV-2 in Belgium. The model is geographically stratified into eleven spatial patches (provinces), and a telecommunication dataset provided by Belgium's biggest operator is used to incorporate the interprovincial mobility. We introduce SARS-CoV-2 variants, seasonality, and vaccines in our model, as their addition has proven necessary for modelling SARS-CoV-2 transmission dynamics during the 2020-2021 COVID-19 pandemic in Belgium. Additionally, we

simulate the model using the Tau-leaping method to account for stochasticity in the transmission of SARS-CoV-2. We calibrate the model using the daily number of hospitalisations in each province and serological data. We demonstrate how our model can be used to help policymakers decide on the optimal timing of the release of social restrictions. We discuss the impact of imposing local mobility or social contact restrictions to shield or contain an epidemic in a given spatial patch and find that lowering social contact is a much better strategy than lowering mobility. We find that incorporating the interprovincial mobility is not necessary to obtain an accurate description of the 2020-2021 SARS-CoV-2 pandemic in Belgium. However, adding spatial heterogeneity by geographically stratifying the model results in scenarios with fewer projected hospitalisation compared to scenarios without a spatial component.

Keywords: SARS-CoV-2 transmission dynamics, compartmental model, spatially explicit, mobility, policy making

1 Introduction

Coronavirus Disease 2019 (COVID-19) is a respiratory disease caused and spread by Severe Acute Respiratory Syndrome Coronavirus 2 (SARS-CoV-2). The virus most likely originated in Wuhan, China in December 2019 [1] and has since spread globally. The pandemic continues up to the moment of writing and is characterised by sequential waves of COVID-19 cases and hospitalisations, warranting a series of preventive governmental policies. Fig. 1 provides a detailed overview of key events and policy changes for Belgium for 2020 and 2021.

To better understand the spread of SARS-CoV-2 in Belgium and inform policymakers, a deterministic, nation-level compartmental model stratified in nine age groups was previously developed [2]. Furthermore, likely future scenarios were bundled and discussed within an interuniversity mathematical modelling consortium named RESTORE. The findings were reported in several policy reports with accompanying press releases [3]. Reflecting the quickly expanding knowledge on COVID-19, the existing model [2] has proven to neatly fit past trends, as well as creating meaningful projections of future trends [4, 5]. The existing national model has been under continuous development as a response to the expanding knowledge on SARS-CoV-2. New knowledge includes firstly detailed information on mobility patterns in Belgium during the 2020-2021 pandemic, secondly the effect of variants of concern (VOCs), seasonality, and vaccines on viral transmissibility and hospitalisation propensity. Finally, the model can benefit from the use of a stochastic solution algorithm. Consequently, we extended the existing model to incorporate these aspects.

The importance of spatial heterogeneity and mobility in Belgium is demonstrated first by the fact that viral spread was not uniform, but rather linked to the location of the initial clusters [6]. Similar conclusions were drawn for France, Italy, and Spain as well [7]. Second, a weak correlation was found between the mobility on the one hand, and the morphology and timing of local COVID-19-related time series on the other hand [6]. Third, a national model cannot take into account local differences in immunity, both natural and due to vaccination, possibly leading to local herd immunity [8, 9]. Fourth, the national model assumes population mixing is spatially homogeneous. This simplifying assumption may result in overestimating future hospitalisation incidence, which may compromise credibility when modelling for policymakers. These four reasons suggest that a Belgian epidemiological model may benefit from the introduction of spatial heterogeneity and mobility, as was successfully done for e.g. Spain [10], Brazil [11] and France [12]. Further, the inclusion of mobility and spatial heterogeneity into the metapopulation models allows scientists to advise policy-makers on the effect of localised measures, by predicting on a local level which areas face imminent danger, as well as which areas play a pivotal role in controlling the spread of the virus [4, 5].

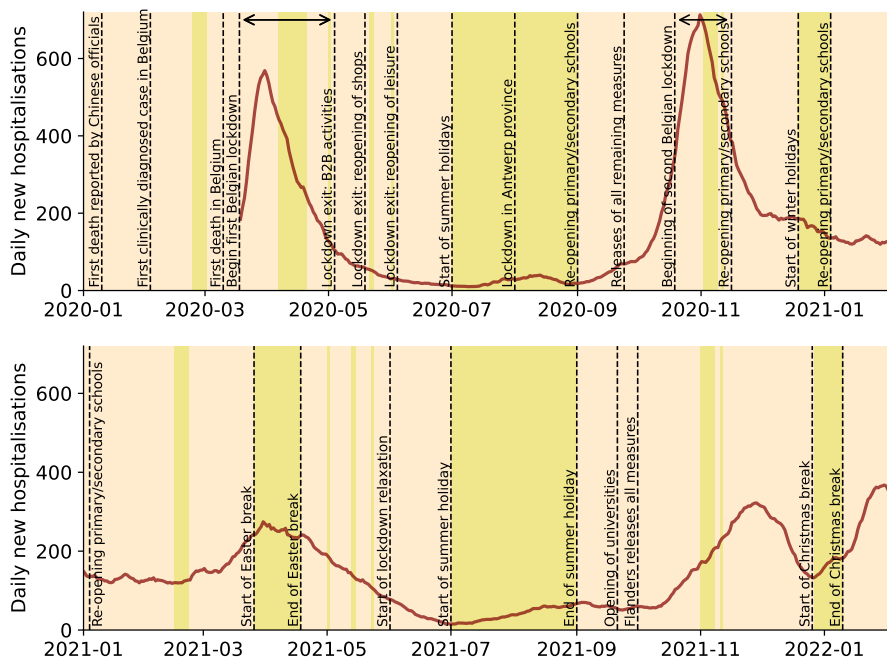


Fig. 1 Seven-day moving average of daily new COVID-19 hospitalisations in Belgium during 2020 and 2021 (maroon line). Vertical dashed lines are used to indicate events or policy changes with a possible impact on social contact behaviour relevant to this work. A green background colour is used to indicate school vacations. The horizontal arrows over the 2020 graph indicate the period of the first and second *strict* lockdown.

The importance of including VOCs and vaccines in the model is motivated by their influence on SARS-CoV-2 dynamics. Subsequent VOCs are associated with different transmissibilities and hospitalisation propensities [13–15], and speculation on increase in severity is an important factor in policy advice [16]. Vaccination has the explicit goal of reducing viral transmission and/or disease severity and has been shown to do this in both clinical trials [17] and society-scale follow-up studies [18]. However, the protection offered by vaccination is imperfect (“leaky”) and was shown to decrease over time, from hereon referred to as *waning* [19]. Furthermore, the protection against severe COVID-19 is more long-lasting than protection against SARS-CoV-2 transmission [18]. In addition, vaccine efficacies differ between VOCs [19]. The direct or indirect effect of seasonal changes on the SARS-CoV-2 transmission rate is not supported by the same overwhelming amount of data due to the limited time since the start of the pandemic. However, seasonality plays a crucial role in many viral diseases [20], and has been required in recent COVID-19 modelling efforts [21].

As explained in more detail in the next section, the Belgian population of 11 million individuals is subdivided in 13 disease compartments, each stratified in 11 provinces, 10 age groups and 4 vaccination states. The large number of compartments results in relatively small populations where stochastic effects may become noticeable [22]. Our previously developed nation-level SARS-CoV-2 model [2] was simulated deterministically because it was stratified in only nine age groups and thus stochastic effects were expected to average out. To simulate the model stochastically, an approximation to the exact Stochastic Simulation Method [23], the so-called Tau-leaping method [24], is used. Instead of simulating each transition between the compartments explicitly, which results in a very small timestep, the Tau-leaping method fixes the length of the timestep at τ and the exact number of transitions in the interval $[t, t + \tau]$ is approximated by a binomial process [25].

In this work, we calibrate the model and demonstrate its adequacy in describing past COVID-19-related time series. Second, we examine the effect of disabling the interprovincial mobility in the model on the description of the past COVID-19-related time series. Third, we demonstrate how the model can be used to set up hypothetical future scenarios to inform policymakers about the effects of social and pharmaceutical policies. Fourth, we compare the difference when the aforementioned scenarios for policymakers are simulated with the national versus the spatially explicit model. Finally, in a purely hypothetical setup, we study if SARS-CoV-2 outbreaks can be contained within a province, or if a province can be shielded from a SARS-CoV-2 outbreak in another province, by imposing local mobility restrictions or social restrictions.

2 Methods

2.1 Disease compartments and stratifications

A compartmental disease model assumes that a population is well mixed and distributed over a number of compartments, each of them corresponding to a stage in the disease development. The model presented here has similar disease compartments as the one we developed previously at nation level for Belgium [2]. A flowchart depicting the various compartments in our COVID-19 model is shown in Fig. 2. The infectious compartment (I) in the original SEIRD formulation [26] is subdivided into nine compartments based on expert knowledge on SARS-CoV-2. In this way, the model accounts for pre-symptomatic and asymptomatic transmission of SARS-CoV-2 [27–29], and for different COVID-19 severities, ranging from mild disease to hospitalisation. Our model distinguishes between regular hospital wards (cohort) and intensive care units (ICUs) and further accounts for a recovery stay in cohort after an ICU stay resulting in a total of 13 disease compartments. Using data from 22 136 COVID-19 patients admitted to Belgian hospitals, we previously obtained the probability of needing intensive care, the mortalities in both hospital wards, and the residence time distributions in both hospital wards [2]. Waning of antibodies (seroreversion) is included, enabling re-susceptibility to SARS-CoV-2 after a prior infection.

Every disease compartment is first stratified into ten age groups: 0-12, 12-18, 18-25, 25-35, 35-45, 45-55, 55-65, 65-75, 75-85 and 85-120 years of age, to account for the fact that social contact and disease severity differs substantially between individuals of different ages [2]. The model is then stratified further in eleven spatial patches representing the 10 Belgian provinces and the Brussels capital region, and four possible vaccination stages: unvaccinated, partially vaccinated, fully vaccinated or boosted. Thus, in total, the model presented here contains $13 \times 10 \times 11 \times 4 = 5720$ states (or metapopulations).

2.2 Stochastic simulation and governing equations

The dynamics shown in Fig. 2 are simulated by iteratively working through two phases: vaccination and disease progress. First, at each subsequent time step $t + \tau$, individuals are transferred between the vaccination metapopulations based on vaccine incidence data. Individuals in the susceptible (S) and recovered (R) disease states are considered eligible for vaccination in the model, and their respective fractions on day t are computed as follows,

$$f_{S,v,i}^g(t) = \frac{S_{v,i}^g(t)}{S_{v,i}^g(t) + R_{v,i}^g(t)}, \quad \text{and}$$

$$f_{R,v,i}^g(t) = 1 - f_{S,v,i}^g(t),$$

where g refers to the spatial stratification, i to the age stratification, and v to the vaccination stage. We assume that vaccines administered between times t

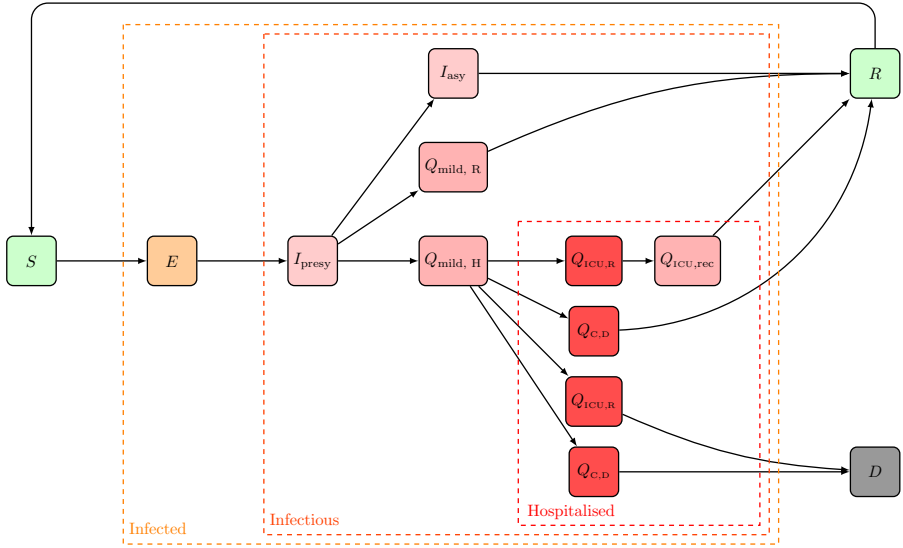


Fig. 2 Flowchart of the SEIQRD model. Here, S stands for susceptible, and E for exposed but not yet infectious. Infected subjects in the I compartments are those that are considered to actively drive the pandemic, because they are either presymptomatic (I_{presy}), or asymptomatic (I_{asy}). Subjects in the Q compartments are assumed not to be infectious, supposedly due to heightened symptom awareness, whether they have mild symptoms ($Q_{\text{mild, R}}$ and $Q_{\text{mild, H}}$), are hospitalised in a regular cohort ward ($Q_{\text{C, R}}$ and $Q_{\text{C, D}}$), are accepted in the ICU ($Q_{\text{ICU, R}}$ and $Q_{\text{ICU, D}}$), or remain in a recovery stay in cohort coming from the ICU ($Q_{\text{ICU, rec}}$). After infection, subjects are either deceased (D) or recovered (R). Recovered subjects may again become susceptible. Every disease state is stratified into 10 age classes, 11 provinces and 4 vaccination states.

and $t + \tau$ are distributed among the susceptible (S) and recovered (R) disease states according to their respective fractions. The number of individuals in province g and age group i entering the new vaccination stage v' between day t and $t + \tau$, is used to compute the vaccine-modified populations of susceptible (S) and recovered (R) individuals,

$$\begin{aligned} \tilde{S}_{i, v'}^g(t) &= S_{i, v'}^g(t) + f_{S, v, i}^g(t)[\phi_{i, v'}^g(t + \tau) - \phi_{i, v'}^g(t)], \quad \text{and} \\ \tilde{R}_{i, v'}^g(t) &= R_{i, v'}^g(t) + f_{R, v, i}^g(t)[\phi_{i, v'}^g(t + \tau) - \phi_{i, v'}^g(t)]. \end{aligned}$$

Here $\phi_{v', i}^g(t)$ is the cumulative number of vaccines of type v' administered in province g and age class i up to times t .

Second, we model the progress of the COVID-19 disease proper, using the Tau-leaping method [24]. The disease dynamics presented in Fig. 2 ultimately involve 17 transitions associated with the following rates (per unit time):

$$\mathcal{R}(\tilde{S} \rightarrow E)_{i, v}^g = \sum_{h=1}^G P^{gh}(t) \sum_w \sum_{j=1}^N \tilde{\beta}_{ij, v w}^{gh}(t)$$

$$\begin{aligned}
& \times \bar{N}_{ij}^{gh}(t) \frac{(I_{\text{presy}}^h)_{j,w,\text{eff}}(t) + (I_{\text{asy}}^h)_{j,w,\text{eff}}(t)}{T_{j,w,\text{eff}}^g(t)} \\
\mathcal{R}(E \rightarrow I_{\text{presy}})_{i,v}^g &= \sigma^{-1}(t) \\
\mathcal{R}(I_{\text{presy}} \rightarrow I_{\text{asy}})_{i,v}^g &= a_i \omega^{-1} \\
\mathcal{R}(I_{\text{presy}} \rightarrow Q_{\text{mild,R}})_{i,v}^g &= (1 - a_i)(1 - h_i(t)) \omega^{-1} \\
\mathcal{R}(I_{\text{presy}} \rightarrow Q_{\text{mild,H}})_{i,v}^g &= (1 - a_i) h_i(t) \omega^{-1} \\
\mathcal{R}(I_{\text{asy}} \rightarrow R)_{i,v}^g &= d_a^{-1} \\
\mathcal{R}(Q_{\text{mild,R}} \rightarrow R)_{i,v}^g &= d_m^{-1} \\
\mathcal{R}(Q_{\text{mild,H}} \rightarrow Q_{C,R})_{i,v}^g &= c_i (1 - m_{C,i}) d_{\text{hospital}}^{-1} \\
\mathcal{R}(Q_{\text{mild,H}} \rightarrow Q_{C,D})_{i,v}^g &= c_i m_{C,i} d_{\text{hospital}}^{-1} \\
\mathcal{R}(Q_{\text{mild,H}} \rightarrow Q_{\text{ICU,R}})_{i,v}^g &= (1 - c_i)(1 - m_{\text{ICU,R}}) d_{\text{hospital}}^{-1} \\
\mathcal{R}(Q_{\text{mild,H}} \rightarrow Q_{\text{ICU,D}})_{i,v}^g &= (1 - c_i) m_{\text{ICU,R}} d_{\text{hospital}}^{-1} \\
\mathcal{R}(Q_{C,R} \rightarrow R)_{i,v}^g &= d_{C,R,i}^{-1} \\
\mathcal{R}(Q_{C,D} \rightarrow D)_{i,v}^g &= d_{C,D,i}^{-1} \\
\mathcal{R}(Q_{\text{ICU,R}} \rightarrow Q_{\text{ICU,rec}})_{i,v}^g &= d_{\text{ICU,R},i}^{-1} \\
\mathcal{R}(Q_{\text{ICU,rec}} \rightarrow R)_{i,v}^g &= d_{\text{ICU,rec}}^{-1} \\
\mathcal{R}(Q_{\text{ICU,D}} \rightarrow D)_{i,v}^g &= d_{\text{ICU,D},i}^{-1} \\
\mathcal{R}(\tilde{R} \rightarrow S)_{i,v}^g &= \zeta
\end{aligned}$$

The meaning and value of all model parameters are listed in Tables [D6](#) and [D7](#). The social contact matrix $\bar{\mathbf{N}}(t)$, the interprovincial mobility matrix $\mathbf{P}(t)$, and the mobility-weighted effective populations of presymptomatic infectious ($\mathbf{I}_{\text{presy,eff}}(t)$), asymptomatic infectious ($\mathbf{I}_{\text{asy,eff}}(t)$) and the total population ($\mathbf{T}_{\text{eff}}(t)$) are time-dependent (see Subsection [2.3](#) and Appendices [A.2](#) and [B](#)). Additionally, the introduction of VOCs, seasonality and vaccination makes the parameters $\tilde{\beta}(t)$, $\bar{h}(t)$, and $\sigma(t)$ time dependent as well (see Subsection [2.4](#) and Appendix [C](#)). Assuming these rates are exponentially distributed, the probability of a single transition from a generic state A to B in province g , age class i and vaccination state v happening between time t and $t + \tau$, is

$$\mathcal{P}(A \rightarrow B)_{i,v}^g = 1 - e^{-\tau \mathcal{R}(A \rightarrow B)_{i,v}^g}.$$

The corresponding number of transitions $A \rightarrow B$ in province g , age class i and vaccination state v between time t and $t + \tau$ are then generated as,

$$\mathcal{N}(A \rightarrow B)_{i,v}^g = \text{Binom}(\mathcal{P}(A \rightarrow B)_{i,v}^g, A_{i,v}^g).$$

Finally, the number of individuals in each of the compartments at time $t + \tau$ is then given by,

$$\begin{aligned}
 S_{i,v}^g(t + \tau) &= \tilde{S}_{i,v}^g(t) - \mathcal{N}(\tilde{S} \rightarrow E)_{i,v}^g + \mathcal{N}(\tilde{R} \rightarrow S)_{i,v}^g, \\
 E_{i,v}^g(t + \tau) &= \mathcal{N}(\tilde{S} \rightarrow E)_{i,v}^g - \mathcal{N}(E \rightarrow I_{\text{presy}})_{i,v}^g, \\
 &\vdots \\
 R_{i,v}^g(t + \tau) &= \tilde{R}_{i,v}^g(t) + \mathcal{N}(I_{\text{asy}} \rightarrow R)_{i,v}^g + \mathcal{N}(Q_{\text{mild,R}} \rightarrow R)_{i,v}^g \\
 &\quad + \mathcal{N}(Q_{\text{C,R}} \rightarrow R)_{i,v}^g + \mathcal{N}(Q_{\text{ICU,rec}} \rightarrow R)_{i,v}^g - \mathcal{N}(\tilde{R} \rightarrow S)_{i,v}^g.
 \end{aligned}$$

The leap value was determined by trial and error and was equal to half a day ($\tau = 0.5 d$).

2.3 Spatially explicit model extension

Interprovincial mobility

Belgium is stratified in a collection of 11 geographical units: 10 provinces and the arrondissement Brussels-capital (NUTS3 level, Fig. A2, Table A1). We will refer to the latter as the ‘11th province’ for convenience. Key to the quantification of interprovincial connectivity is the telecommunication dataset provided by Belgium’s largest telecom operator Proximus (Appendix A.2). The use of this type of data as a proxy for mobility has been shown to be legitimate [30], and has been done in the particular context of COVID-19 in other analyses and modelling efforts [31–33]. The geographical spread of subjects between G provinces is quantified in a $G \times G$ time-dependent mobility matrix $\mathbf{P}(t)$ with elements $P^{gh}(t)$. Element $P^{gh}(t)$ represents the estimated fraction of all the time available to all subjects in province g , spent in province h , in the day corresponding to time t . Fig. 3 schematically depicts the mobility between three provinces. As an example, two time series of $P^{gh}(t)$ for two different (g, h) pairs are shown in Fig. 4.

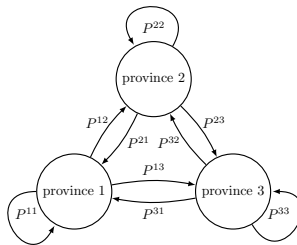


Fig. 3 Schematic representation of the interpretation of the inter-provincial mobility matrix \mathbf{P} for only three provinces. In the model we consider 11 Belgian provinces, and the mobility matrix elements are time-dependent (Fig. 4).

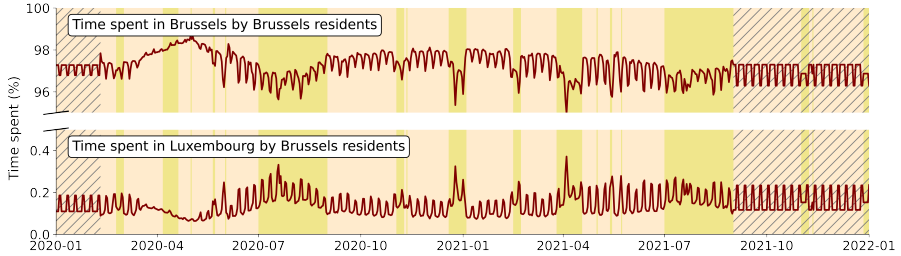


Fig. 4 Two of the 11^2 time series $P^{gh}(t)$, here representing the daily percentage of time that all residents of Brussels spent in their home province (top), or in Luxembourg province (bottom). The hatched regions indicate periods for which an estimation was made, because no data was available.

The mobility matrix $\mathbf{P}(t)$ is used to determine the number of susceptible people from province g that visit province h at time t , and the *effective* population sizes per model compartment in the visited province h [10]. Mathematically, the effective population size is computed as follows:

$$X_{i,v,\text{eff}}^g(t) = \sum_{h=1}^G P^{hg}(t) X_i^h, v(t), \quad (1)$$

where X is a generic disease state. Daily effective population is calculated for states $\mathbf{I}_{\text{presy}}$ and \mathbf{I}_{asy} , and for the total population \mathbf{T} .

Provincial social contact

The number of social contacts depends on the geographical location in two ways. First, prepandemic contact matrices are scaled with activity indicators at the Belgian provincial level (see Appendix B). Second, the types of social contact differ depending on whether or not an individual is in their home province. We assume that one only has work-related contacts in visited provinces, whereas all types of contact are possible within the home province. The size and time dependence of the social contact matrix results from multiplying four factors and summing over six locations, i.e.

$$\widetilde{\mathbf{N}}^g(t) = \sum_{k \in \text{loc}} M(t) \Omega^k G^{k,g}(t) \mathbf{N}^k, \quad (2)$$

with elements $\widetilde{N}_{ij}^g(t)$ representing the average daily number of contacts at time t between subjects in age class i and j , in province g . The sum is over locations that are associated with distinct average contact behaviour: home, school, work, transport, leisure, and other. \mathbf{N}^k is a prepandemic social contact matrix taken from the SOCRATES web tool [34] and based on a 2010-2011 social contact survey conducted in Flanders that was revisited recently in the context of COVID-19 [35]. The observational time series $G^{k,g}(t)$ are taken from the Google Community Mobility Reports (GCMRs) [36] and constitute the

primary tool for rescaling the prepandemic social contact matrices. These data are available daily at the Belgian provincial level since February 15th 2020, and quantify the “activity” in different locations compared to a prepandemic baseline. Ω^k , from hereon referred to as the “effectivity” of a contact in location k was introduced because the effectivity of a contact in a given location depends on a combination of the physical proximity and the duration of the contact, which we expect is different from location to location. Alternatively, it can be seen as the degree correlation between the Google mobility indicator in location k and reductions in the spread of SARS-CoV-2. A low value of Ω_k suggests a change in the Google mobility indicator has a limited effect on viral transmission, i.e. the Google indicator is inadequate. Although six effectivities could be introduced for the six locations, we introduced only two based on expert knowledge and Sobol sensitivity analysis, namely $\Omega^{\text{work, schools}}$ and Ω^{rest} , where the former results from lumping the effectivities of leisure, transport, and other contacts, and the latter from lumping the effectivities of workplaces and schools. The effectivity of Ω^{home} was assumed to equal one. The values of Ω^{rest} and $\Omega^{\text{work, schools}}$ are obtained during model calibration.

Finally, a mentality factor $M(t)$ was added to the social contact model because preliminary research indicated that public awareness to SARS-CoV-2 triggers an apparent mentality change that reduces the number of social contacts further than the GCMRs data suggest. The mentality factor is introduced twice when lockdown measures were taken and is subsequently released twice over a two-month period after the first lockdown measures were eased. The value of $M(t)$ is obtained during model calibration. Two examples of resulting time series $\tilde{N}_{ij}^g(t)$ are shown in Fig. 5. Combining the above, the linear combination of prepandemic interaction matrices used to model pandemic social contact becomes

$$\begin{aligned} \tilde{\mathbf{N}}^g(t) = & \mathbf{N}^{\text{home}} + M(t) \left\{ \Omega^{\text{work, schools}} \left[\mathbf{G}^{\text{schools,g}}(t) \mathbf{N}^{\text{schools}} + \mathbf{G}^{\text{work,g}}(t) \mathbf{N}^{\text{work}} \right] \right. \\ & \left. + \Omega^{\text{rest}} \left[\mathbf{G}^{\text{transport,g}}(t) \mathbf{N}^{\text{transport}} + \mathbf{G}^{\text{leisure,g}}(t) \mathbf{N}^{\text{leisure}} + \mathbf{G}^{\text{other,g}}(t) \mathbf{N}^{\text{other}} \right] \right\}. \end{aligned} \quad (3)$$

Additional details concerning the social contact model can be found in Appendix B. Since we assumed that only work-related contacts are possible in visited provinces, whereas all types of contact are possible within the home province, we express the social contact of an average subject from province g visiting province h as

$$\bar{\mathbf{N}}^{gh}(t) = \delta^{gh} \tilde{\mathbf{N}}^g(t) + (1 - \delta^{gh}) M(t) \Omega^{\text{work}} \mathbf{G}^{\text{work,h}}(t) \mathbf{N}^{\text{work}}, \quad (4)$$

where δ^{gh} is the Kronecker delta.

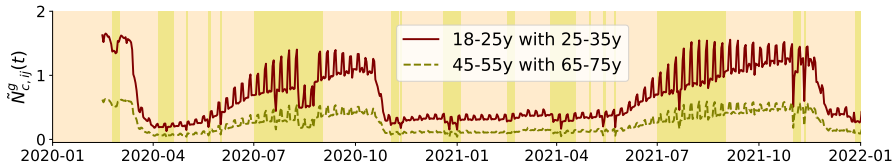


Fig. 5 Example of time series $\tilde{N}_{ij}^g(t)$ for Brussels, which represent the local effective social contact between two age classes i and j . These series result from the multiplication of four factors shown in Eq. (2). The solid maroon curve shows effective contact between 18-25 year-olds and 25-35 year-olds. The dashed olive curve shows the same information, but 45-45 year-olds contacting 65-75 year-olds, clearly following a similar overall trend but involving fewer contacts.

Population density dependence

We assume that average population density affects the effective transmission coefficient (similar to [10]). We define three different transmission coefficients based on the population density. Essentially, this turns β into a vector with three degrees of freedom,

$$\beta \rightarrow \boldsymbol{\beta} \text{ with elements } \beta^g \in \{\beta^R, \beta^U, \beta^M\}, \quad (5)$$

depending on whether we consider the province g to be predominantly rural, urban, or metropolitan (see Table A1).

2.4 Dynamical rescaling of model parameters to include VOCs, seasonality, and vaccines

Variants of concern

Beyond the wild-type SARS-CoV-2 variant, we consider four VOCs identified by the World Health Organisation [37]: Alpha, Beta, Gamma, and Delta. Due to their similar properties in our model [38], we aggregate the first three VOCs, denoted as α - β - γ . To model the emergence of these variants, national prevalence data were used [39] (see Fig. C6, top). At every time t , a weighted average infectiousness of SARS-CoV-2 variants was computed using the variant fractions, which effectively turns the (geographically stratified) transmission coefficient into a time-dependent function, i.e.

$$\beta(t) = \beta \sum_n \alpha_n(t) K_{\text{inf},n}. \quad (6)$$

Here $\alpha_n(t)$ represents the fraction of variant n present in Belgium at time t , and $K_{\text{inf},n}$ is the increase in infectivity compared to the wild type, whose distributions are determined during the calibration procedure. The variants were assumed to alter the serial interval and disease severity as well, which translates to dynamically changing the length of the average latent time (σ) and the hospitalisation propensity (\mathbf{h}) in a similar fashion (see Fig. C6, bottom). The

latter rescaling parameters are derived from literature [13–15, 40] and listed in Table C2.

Seasonality

Changes in climate have been recognised to play a role in the spread of many viral diseases amongst humans, notably influenza [20]. Seasonality is included in our model by scaling the transmission coefficient of SARS-CoV-2 with a cosine function [21]. Its period is one year, and its amplitude is denoted by A , i.e.

$$\bar{\beta}(t) = \beta(t) \left[1 + A \cos \left(2\pi \frac{t}{365 \text{ days}} \right) \right]. \quad (7)$$

Here t is expressed in days since January 1st, at which time we assume the $\bar{\beta}(t)$ values are maximal. Its simplicity reflects the current lack of understanding of seasonality’s actual effect on SARS-CoV-2, mainly due to lack of long-term data. The amplitude A is determined during the calibration procedure.

Vaccination

Vaccine incidence data are publicly available for all Belgian provinces and per age class [41]. The fraction of individuals in the population with a partial, full, or boosted vaccination is shown in Figs. C8 and C9 of the supplementary materials. As shown in Subsection 2.2, cumulative vaccination data $\phi_v(t)$ are used to transfer people between vaccination stages. These data can be further exploited to estimate the effective (average) protection people in vaccination stage v experience at time t , as we elucidate below.

In every vaccination state, the vaccine is assumed to offer protection through three mechanisms: 1) Vaccines lower the susceptibility to SARS-CoV-2, 2) Vaccines lower the infectiousness of an individual infected with SARS-CoV-2, 3) Vaccines lower the hospital admission propensity of COVID-19. To incorporate the effect of *waning* vaccine immunity, the vaccine efficacies within each vaccination metapopulation are rescaled dynamically based on vaccination history. This approach is preferred over adding more vaccination states to limit the computational burden, optimally use the available vaccine incidence data, and allow the three vaccine efficacies to wane at different rates, which decrease to zero, which is not possible using a metapopulation approach.

We compute dynamic vaccine efficacies $\mathbf{E}_{v,n,\text{susc}}(t)$, $\mathbf{E}_{v,n,\text{inf}}(t)$ and $\mathbf{E}_{v,n,\text{hosp}}(t)$ for every vaccine stage v , VOC n (and age group i and province g) assuming exponential waning of the vaccine. For that purpose, we rely on 1) the past vaccine incidence, available per province g , age group i and vaccination stage v [41], 2) the vaccine efficacies for every protective mechanism, vaccination stage v and every VOC n , both 25 and 175 days after vaccination (see Table C3) [19], and 3) the assumption that waning is governed by a

decreasing exponential,

$$\tilde{E}_{v,n,\text{susc}}(t) = E_{v,n,0,\text{susc}} \exp(-t/l), \quad (8)$$

where,

$$l = \frac{150 \text{ d}}{\ln\left(\frac{E_{v,n,0,\text{susc}}}{E_{v,n,w,\text{susc}}}\right)} > 0, \quad (9)$$

and similarly for $\tilde{E}_{\text{full},n,\text{inf}}(t)$ and $\tilde{E}_{\text{full},n,\text{hosp}}(t)$ (see Fig. C7). These waning functions can be combined with the (previously administered) vaccines to compute the weighted average vaccine efficacy in province g and age class i at time t as follows,

$$\mathbf{E}_{v,n,\text{susc}}(t) = \frac{1}{\phi_v(t)} \int_{-\infty}^t \dot{\phi}_v(t') \tilde{E}_{v,n,\text{susc}}(t-t') dt', \quad (10)$$

where $\dot{\phi}_v(t)$ is the time derivative of the *cumulative* number of individuals that reached vaccination stage v at time t for the various age and province populations. Hence, when a large number of individuals are vaccinated to vaccination stage v at once, the average vaccine efficacy in that metapopulation will temporarily increase. The efficacies $\mathbf{E}_{v,n,\text{susc}}$ and $\mathbf{E}_{v,n,\text{inf}}$ are then used to scale the transmission coefficient,

$$\bar{\beta}_{vw}^g \rightarrow \bar{\beta}_{vw}^g \text{ with elements } \bar{\beta}_{ij,vw}^{gh} = \bar{\beta}^g \sum_n \alpha_n(t) (1 - E_{v,n,\text{susc},i}^g) (1 - E_{w,n,\text{inf},j}^h), \quad (11)$$

Similarly, the values $\mathbf{E}_{v,\text{hosp}}(t)$ scale the hospitalisation propensities (\mathbf{h}). An overview of all parameters introduced as part of a time-dependency of the parameters $\tilde{\mathbf{N}}(t)$, $\beta(t)$ and $\mathbf{h}(t)$ are summarised in Table D7.

2.5 Model calibration

Calibrated parameters

Nine model parameters are considered to be a priori unknown and must be calibrated using the available data: 1-3) The probabilities of infection upon contact with an infectious individual (β^R , β^U and β^M), 4-5) The effectivities of contacts in schools and in workplace, and during leisure activities ($\Omega^{\text{work,schools}}$, Ω^{rest}), 6) The additional reduction of the contacts under lockdown measures, which could not be explained by activity reductions observed in the GCMR, named “mentality“ (M), 7-8) The infectivity gains of the relevant VOCs ($K_{\text{inf},\alpha\beta\gamma}$, $K_{\text{inf},\delta}$) and 9) The seasonal amplitude of the infectiousness (A). The simulated daily number of hospitalisations is matched to the eleven time series of daily new hospitalisations in each province, starting on March 15th, 2020 and ending on October 14th, 2021. Further, assuming that on average half of the

recovered subjects are again susceptible after one year (associated with seroreversion rate parameter ζ), the simulated numbers of recovered individuals are matched to seven serological measurements from Herzog et al., 2020 [42] and 21 serological measurements from Sciensano [43], spanning the period from March 30th, 2020 until January 8th, 2021.

Initial condition

To find an appropriate initial condition on March 15th, 2020, the model was initialised on February 5th, 2020, corresponding to the day the first case was detected in Belgium. The model was simulated without seasonality or mobility, with all effectivities set to one, and with a reproduction number of $R_0 = 3.3$ (corresponding to all $\beta^g = 0.027$). The number of initial infected that resulted in the best fit to the provincial time series between March 15th, 2020 and March 22nd, 2020 was determined. The model states on March 15th, 2020 were then used as the initial condition.

Statistical model

We found that a quadratic relationship best describes the relationship between the mean and variance of the daily hospitalisations time series data, indicating that a negative binomial model is best fit to describe the relationship between the model outcome and observed data [44] (see Appendix E.1). We therefore iteratively optimise the following log-likelihood function,

$$\log \mathcal{L}(\tilde{\mathbf{x}}|\mathbf{x}) = - \sum_{g=1}^G \sum_{t=1}^n \left(\log \left[\frac{\Gamma(x_t^g + 1/\alpha^g)}{\Gamma(x_t^g + 1)\Gamma(1/\alpha^g)} \right] + \frac{1}{\alpha^g} \log \left[\frac{1/\alpha^g}{1/\alpha^g + \tilde{x}_t^g} \right] + x_t^g \log \left[\frac{\tilde{x}_t^g}{1/\alpha^g + \tilde{x}_t^g} \right] \right). \quad (12)$$

Here the outer sum is over all $G = 11$ provinces. The inner sum is over all n observed data points at times t . Γ is the gamma function. $\tilde{\mathbf{x}}$ represents the simulated time series of daily hospitalisations (obtained by summing over all age groups and vaccination states), and \mathbf{x} the equivalent observed time series. By fitting the negative binomial model to the mean-variance relation of the provincial time series, the overdispersion parameter α^g , which quantifies the presumed error on the data per province g , was computed and subsequently used in the optimisation procedure (see Table E9). Maximising the result of Eq. (12) is computationally demanding and has local minima. A good technique to initially broadly identify the region where the global maximum is situated is Particle Swarm Optimisation (PSO) [45]. Subsequently, once a region of interest has been identified, we use the maximum-likelihood estimates as initial values for the ensemble sampler for Markov Chain Monte Carlo (MCMC) [46]. For all parameters, uniform prior distributions were used. More details are found in Appendix E, and section 3.1 contains calibration results.

2.6 Scenario analyses

2.6.1 Scenarios for policymakers

Next, we illustrate how our model can be used to simulate the combined impacts of the emergence of new variants, an ongoing nation-wide vaccination campaign and social relaxations. Such simulations can be used to provide policymakers with insights on the optimal timing of the release of social restrictions. We therefore calibrate our model up to March 1st, 2021, a point in time interesting because the α - β - γ VOCs had just become dominant, the Belgian vaccination campaign was picking up speed, and there was a high pressure to relax social restrictions. Under the emergence of the α - β - γ VOCs and vaccination campaign, we thus define four future scenarios in which social restrictions are released.

The first scenario (S0) assumes that social restrictions are gradually eased over a two-month period, starting on March 1st, 2021. The subsequent scenarios S1 through S3 then postpone the release date of the social restrictions by one month. Thus, measures are released on April 1st, May 1st and June 1st for scenarios S1 through S3. In all scenarios, we assume that the Delta variant does not emerge and the observed number of administered vaccines are used. The number of vaccine doses that would be administered was of course not known on March 1st, 2021, but in policy advice given at that time, realistic projections for the future-administered doses were used. The scenarios are additionally simulated using our equivalent nation-level model to demonstrate the effect of adding spatial heterogeneity on the outcome of these scenarios. The (total) number of contacts associated with each scenario is shown in Fig. 6).

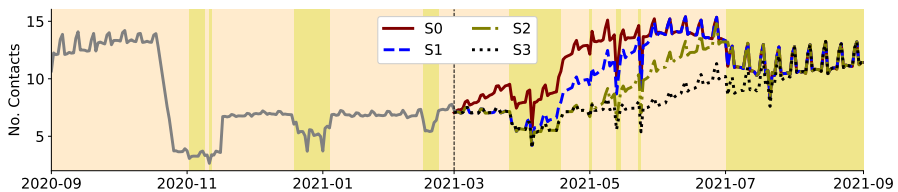


Fig. 6 Age-weighted average of the observed social contact matrix elements $N_{ij}(t)$ (grey), plotted alongside the social contact associated with scenarios S0 (release of social restrictions on March 1st, 2021), S1 (April 1st, 2021), S2 (May 1st, 2021), and S3 (June 1st, 2021).

2.6.2 Spatially explicit scenarios

A particular strength of our model is its ability to explore the impact of mobility restrictions on the spread of SARS-CoV-2 in Belgium. We inspect if altering the mobility between two provinces can be used to contain an epidemic within a province, or alternatively, if altering the mobility between two provinces can

shield one province from an epidemic in the other. Next, we assess in a similar manner the impact of limiting social contacts in one of the provinces. All simulations are started on January 1st 2020, upon which we inspect the resulting hospitalisations until September 1st, 2020. In all scenarios, seasonality, VOCs and vaccines are omitted. Default social contact and mobility are equal to their pre-pandemic values. Due to their large demographic differences and their relatively weak connectivity, we inspect results for Brussels and Luxembourg.

Regulating local mobility

We define a parameter \mathbf{p} whose elements $p^g \in [0, 1]$ linearly control the mobility to and from province g , compared to some static baseline mobility,

$$\bar{\mathbf{P}} = \text{avg} \{ \mathbf{P}(t) \} \quad \text{for } t < \text{March 15th 2020.} \quad (13)$$

the values p^g are defined implicitly as

$$\tilde{p}^{gh} = \bar{P}^{gh} p^g p^h + \delta^{gh} \sum_{f=1}^G \bar{P}^{gf} (1 - p^f p^h), \quad (14)$$

where δ^{gh} is the Kronecker delta. We assume social contact behaviour remains the same and is independent of whether a province is a subject's home province or a visited province. We change the connectivity between Brussels and Luxembourg to *shield* Brussels from an outbreak in Luxembourg (Mob. S.), or we attempt to *contain* an outbreak in Brussels (Mob. C.). The simulations are started with 10 exposed individuals, distributed over the model's 10 age groups according to the demographics of the spatial patch. In Mob. S., the index patients are in Luxembourg, while in Mob. C., the index patients are in Brussels. We run the simulation 100 times for each of the 30 p^g values logarithmically spaced between 1 and 10^{-3} . Because of the stochastic nature of the model, in the analysis, the mean of the 100 repeated simulations is used.

Regulating local social contact

We define a parameter \mathbf{n} whose elements $n^g \in [0, 1]$ determine the local average social contact compared to the pre-pandemic baseline social contact \mathbf{N} :

$$\bar{N}_{ij}^{gh}(t) = n^g (N_{ij} - N_{ij}^{\text{home}}) + N_{ij}^{\text{home}}. \quad (15)$$

Note that this quantity is independent of the province of origin g : thus, for work contacts, subjects follow the social rules of the province they *visit*. By altering the social contacts in Brussels, we perform a similar analysis for shielding and containing an initial outbreak in Brussels or Luxembourg. We call these scenarios Soc. S. and Soc. C., respectively. We again run 30 (times 100) simulations, one for every n^g value, now equidistantly spaced between 1 and 0, and all other parameters are fixed (including mobility $\mathbf{p} = 1$).

3 Results and discussion

3.1 Model calibration

We show the nationally and regionally aggregated simulations between March 15th and October 14th 2021 in Fig. 7. In Figs. E13 and E14, we show the fit of the calibrated model to each of the eleven provincial time series. In Fig. 8 we show the (absence of) differences in the time series of the negative binomial log-likelihood score between the observed and simulated daily new hospitalisations of the spatially explicit model when interprovincial mobility is included or excluded. In Fig. E16, we show the nationally aggregated fit to the seroprevalence data. Further, we show a corner plot with the posterior distributions of the 9 calibrated parameters in Fig. E12. All calibrated parameter values are listed in Table E10. The time series of the negative binomial log-likelihood score between the observed and simulated daily new hospitalisations of the spatially explicit model are given in Fig. E15, alongside the ones of the previously established national model [2].

Goodness-of-fit

In general, over the calibrated period (before the dashed line in Fig. 7), both the regional and national aggregates fit the observed number of daily hospitalisations well (Fig. 7). Beyond the model’s calibration period (after the dashed line in Fig. 7) during the Delta wave of October-December 2021, the forecasted number of new hospitalisations is adequate at the national level. However, upon examination of the regional breakdown of the forecast, the daily hospitalisations during the Delta wave are slightly underestimated in Flanders, slightly overestimated in Wallonia, and severely overestimated in Brussels. There were large differences in the regional vaccination degree prior to the Delta wave, Flanders (91.4% of 18+ by October 1st 2021) has a much higher vaccination coverage than Wallonia (79.8%) and Brussels (66.5%) (see Fig. C8). Based on the vaccine coverage, one would expect Brussels to experience the highest and Flanders to experience the lowest Delta hospitalisation wave, But Flanders saw the highest Delta wave. We offer two explanations for this contra-intuitive observation. First, the vaccines might have waned faster or their efficacy against the Delta VOC might have been lower than reported which would result in the mitigation of the effects of regional differences in vaccine coverage. Second, prior to the Delta wave, there were still some social restrictions in Wallonia and Brussels, while the Flemish government had released all measures already on October 1st, 2021. In spite, no difference in the degree of social contact was observed in the GCMRs, so the expected difference in social contact was not adequately captured by our social contact model. Survey-based contact studies under lockdown measures at the regional level could have been used to explain the regional difference in Delta peak height. This highlights that our model’s regional predictions are only as good as the regional contact data used as an input. The spatially explicit model is

inherently more data-hungry than its national counterpart.

Figure 8 shows the differences in the time series of the negative binomial log-likelihood score between the observed and simulated daily new hospitalisations of the spatially explicit model with and without inclusion of interprovincial mobility. No significant difference in goodness-of-fit was found, so the interprovincial mobility does not have a significant impact on the model outcome during the calibration period. A likely explanation is simulations were started on 2020-03-15, when SARS-CoV-2 was already widely spread in the general population. The impact of interprovincial mobility is likely mitigated because SARS-CoV-2 was constantly present in every Belgian province over the calibrated range. From these results, we conclude that incorporating interprovincial mobility in Belgium was not necessary to obtain an accurate description of the 2020-2021 SARS-CoV-2 pandemic in Belgium. This finding is consistent with the work of Rollier et al. [6], who concluded that the overall correlation between the shape and timing of epidemic peaks in two arrondissements and the mobility between them was in general weak for SARS-CoV-2 in Belgium. The correlation was strongest during epidemic onset but quickly declined once the epidemic became widespread.

Calibrated parameter values

The values and 95% quantiles of the calibrated parameters are listed in Table E10 and shown in more detail in Fig. E12. Some noteworthy values are discussed here. Even though the calibrated values for the transmission coefficients for rural or urban provinces are rather similar, the metropolitan β^M value (0.024 ± 0.002) is significantly larger than its rural β^R and urban β^U counterparts (0.021 ± 0.002). It appears that Brussels, with its *much* larger average population density, accommodates an increased effective viral transmission. The calibrated effectivity parameters Ω^k have well-resolved and distinct values. The effectivity for contacts in the workplace and in schools (0.49 ± 0.13) is slightly lower than those of leisure contacts (0.64 ± 0.23). This indicates that the daily number of hospitalisations in Belgium is most sensitive to changes in the leisure mobility in the GCMRs. We found a mentality value of $M = 61 \pm 5\%$ during the time periods indicated in Fig. B5, corresponding to periods of sustained lockdown measures. This indicates that during these periods, a 39 % *additional* reduction in social contacts is needed to model the epidemic as compared to periods when SARS-CoV-2 poses no imminent threat. Important is the non-zero value for the seasonality amplitude. Since $A = 19 \pm 4\%$ this implies that SARS-CoV-2 is 46% more transmissible during winter compared to summer time. The increases in SARS-CoV-2 infectivity $K_{\text{inf},\alpha\beta\gamma}$ and $K_{\text{inf},\delta}$ due to VOCs are significant. We find respectively a $28 \pm 9\%$ and a $61 \pm 11\%$ increase as compared to the wild-type variant.

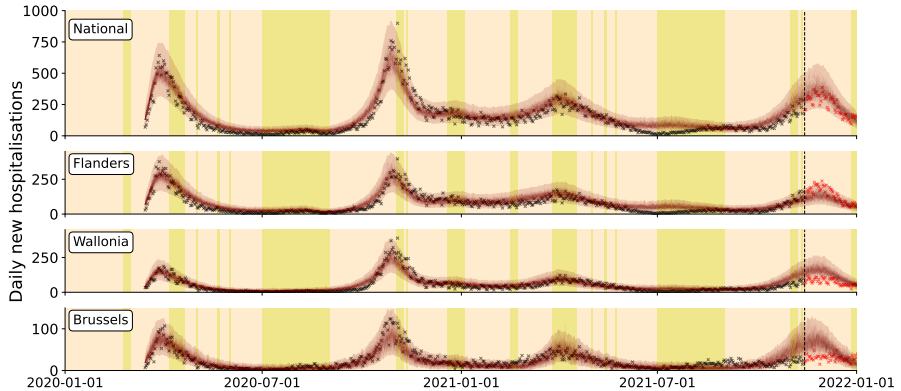


Fig. 7 100 model realisations of the daily new hospitalisations between March 15th 2020 and January 1st 2022 (solid lines) with a negative binomial 95% confidence region (transparent band). Black crosses signify raw data from Sciensano [43] were used in the calibration procedure while red crosses signify data were not used during the calibration procedure. From top to bottom: Nationally aggregated daily number of hospitalisations, daily hospitalisations aggregated over all Flemish provinces, daily hospitalisations aggregated over Walloon provinces, daily hospitalisations in Brussels (see Table A1 and Fig. A2).

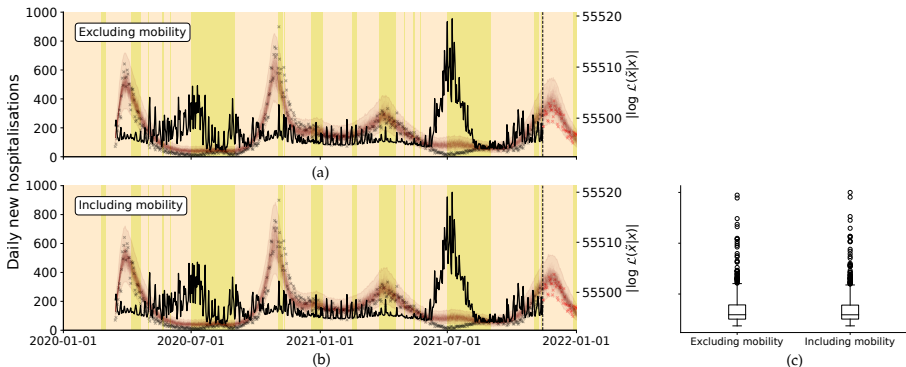


Fig. 8 100 realisations of the daily new hospitalisations between March 15th 2020 and January 1st 2022 using the spatially explicit model (a) excluding interprovincial mobility and (b) including interprovincial mobility. The accompanying negative binomial log-likelihood score of the model predictions is given in black on the right hand axis. (c) Boxplot of the log-likelihood values at every time t .

3.2 Scenario analyses

3.2.1 Scenarios for policymakers

We start by focusing on the provincial-level model first (top panel, Fig. 9). If the measures are released on March 1st (S0), the provincial model predicts a peak of 1000 daily hospitalisations by the first week of June, surpassing the 800 daily hospitalisations of the second 2020 COVID-19 wave. Relaxing measures on April 1st (S1) results in a peak of 500 hospitalisations per day by July 1st, 2021. Although the hospitalisation peak of S1 seems less threatening,

the total number of hospitalised patients, equal to the area under the curve of daily hospitalisations, would severely strain if not completely disrupt the Belgian healthcare system. Relaxations starting on May 1st, 2021 (S2) and June 1st, 2021 (S3) contain the epidemic, likely due to the combined effect of vaccination and favourable seasonal changes during summer. Our projections strongly recommend against the relaxation of social relaxations on March 1st (S0), and on April 1st (S1), *even* if the measures are gradually relaxed over a two-month period. Relaxations are possible starting May 1st (S2). In reality, measures were relaxed starting mid May 2021, corresponding to a situation roughly between S2 and S3.

We then shift our attention the nation-level model (bottom panel, Fig. 9). The peaks in daily hospitalisations are much higher than those projected by the spatially explicit model and are associated with much lower uncertainty. Further, based on the projections of the nation-level model, it may seem beneficial to postpone relaxations until June 1st (S3).

These results illustrate that despite the interprovincial mobility not affecting the model outcomes under high SARS-CoV-2 prevalences, adding spatial heterogeneity can still be beneficial by providing less pessimistic projections. It also illustrates that models should be interpreted with care and if possible, results from different models should be combined in an ensemble to increase the robustness of the predictions [3, 16]. Relying on such an ensemble gives more weight to the overall trends in the policy advice than to the quantitative model outcomes, which are (in our experience) disproportionately focused on by policymakers and press media.

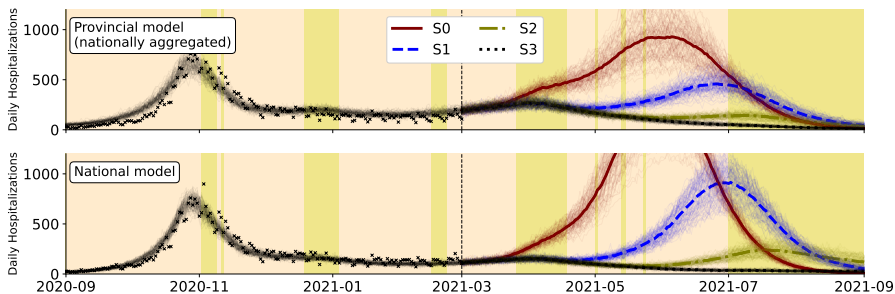


Fig. 9 Combined impact of the α - β - γ VOCs, the ongoing nation-wide vaccination campaign and social relaxations on the number of daily hospitalisations. Social relaxations start on March 1st, 2021 (S0), and are postponed by one month in the other scenarios. The result of 100 stochastic simulations and their mean are shown. *Top*: Simulated using the provincial-level model. *Bottom*: Simulated using the (equivalent) nation-level model.

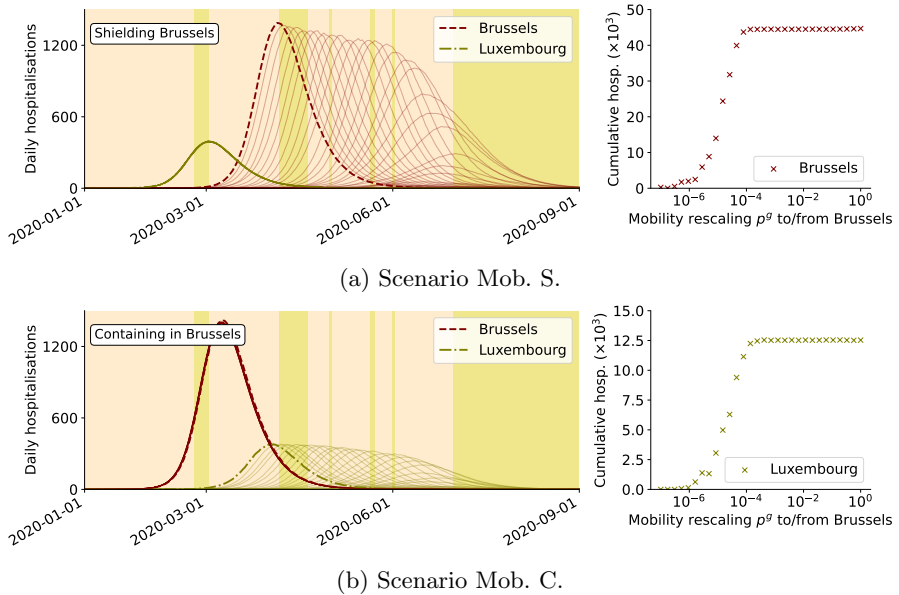


Fig. 10 Effect of decreasing mobility between Brussels and Luxembourg on 30 simulated hospitalisation time series, either when (top) shielding Brussels from an outside epidemic, simulated as 10 index patients introduced in Luxembourg or (bottom) containing an epidemic within Brussels, simulated as 10 index patients introduced in Brussels.

3.2.2 Spatially explicit scenarios

Regulating local mobility

In scenario Mob. S. (Fig. 10(a)), where we attempt to shield Brussels from an epidemic originating in Luxembourg, for all practical isolation cases, the effect of lowering the mobility is to *delay* the onset of the epidemic in Brussels without lowering the cumulative number of hospitalisations. Only when extreme isolation values of $p^g < 10^{-4}$ are reached, which correspond to single commuters between these provinces, does the expected cumulative number of hospitalisations decline. In scenario Mob. C. (Fig. 10(b)), where we attempt to prevent an epidemic originating in Brussels to spread to Luxembourg, a similar result is obtained. During the first, very strict national lockdown, the corresponding value for p^g was approximately 0.5, (see Fig. 4). Consequently, we may conclude that *only* reducing mobility can delay the spread of a SARS-Cov-2 epidemic but can ultimately not contain it. The qualitative relations are of course not unique to Brussels and Luxembourg, but apply to all pairs of provinces.

Regulating local social contact

In scenario Soc. S. (Fig. 11(a)) we attempt to shield Brussels from an epidemic originating in Luxembourg by lowering social contact in Brussels. Reducing social contact in Brussels does not influence the epidemic in Luxembourg,

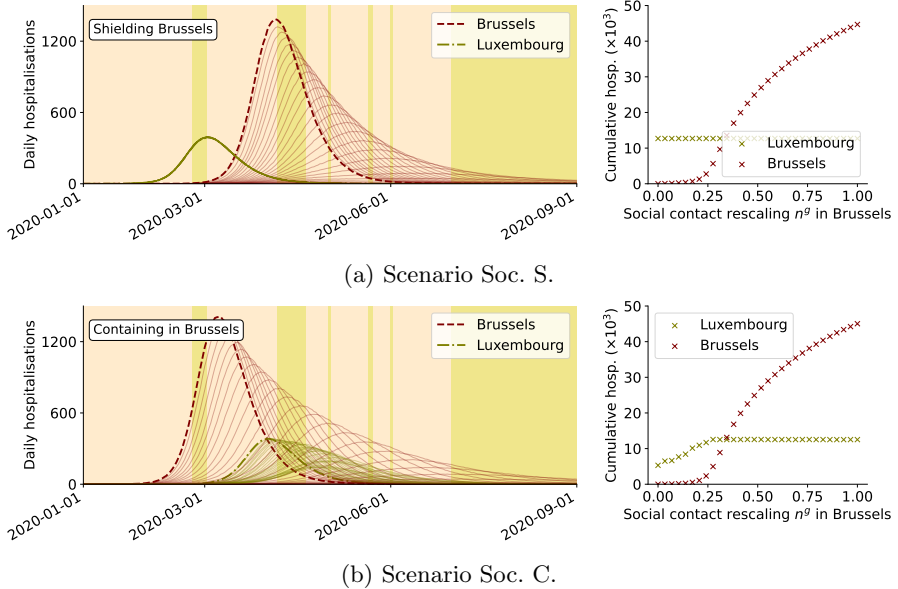


Fig. 11 Effect of decreasing social contact in Brussels on 25 simulated hospitalisation time series, either to (top) shield Brussels from an outside epidemic, simulated as 100 index patients introduced in every age class in Luxembourg or to (bottom) contain an epidemic within Brussels, simulated as 100 index patients introduced in every age class in Brussels.

while strongly delaying *and* reducing the epidemic in Brussels. Especially for $0.25 < n^g < 0.50$, a strong decrease in the expected cumulative number of hospitalisations occurs in Brussels. In the containment scenario Soc. C. (Fig. 11(b)) we attempt to prevent an epidemic originating in Brussels from spreading to Luxembourg by lowering social contacts in Brussels. A similar trend as in scenario Soc. S. is seen for Brussels. However, we observe an additional effect of *delaying* and, for large social contact reductions ($n^g < 0.25$) in Brussels, lowering the expected cumulative number of hospitalisations in Luxembourg. The epidemic in Luxembourg is never fully contained by lowering social contact in Brussels and this is a consequence of the way the scenario is setup. If $n^{\text{Brussels}} = 0$ but $p^{\text{Brussels}} = 1$, Brussels residents are still commuting to other provinces where they have their work contacts, hence the epidemic can, in a fraction of the 100 simulations, still spread across Belgium. From these scenarios we conclude that lowering social contacts is a much more effective policy measure than lowering mobility to contain a SARS-COV-2 epidemic.

4 Conclusions

Starting from our previously developed national model [2], we developed a spatially explicit model variant which we then simulated stochastically. Both models were, over the past two years, extended to account for the emergence of VOCs, seasonality, and vaccines. These were critical model additions that

A Stochastic Mobility-Driven Spatially Explicit SEIQRD COVID-19 Model with VOCs, Seas

were desired and required for the description, forecasting and understanding of the COVID-19 pandemic in Belgium.

We have demonstrated the spatially explicit model's ability to describe the relevant COVID-19 time series in Belgium. We then demonstrated its capabilities to evaluate scenarios on the effects of non-pharmaceutical policy interventions, which can – and have been – applied to support the pandemic decision-making process. In addition, we used the model to study the effects of locally reducing mobility and of locally reducing social contact to shield or contain an epidemic and found that lowering social contact is a more effective means of containing a SARS-CoV-2 epidemic than lowering mobility.

Additionally, we assessed if adding the impact of spatial heterogeneity and interprovincial mobility is worth the added complexity. This question is of importance when deciding which model to use; its answer is nuanced and depends on the intended purpose. First, we have assessed the differences in goodness-of-fit over the calibrated range with and without the inclusion of interprovincial mobility and found that incorporating interprovincial mobility in Belgium was *not* necessary to obtain an accurate description of the 2020-2021 SARS-CoV-2 pandemic in Belgium. Second, when modelling scenarios for policymakers, adding spatial heterogeneity into the model has a pronounced impact: 1) It relaxes the assumption of homogeneous mixing at the national level and this results in fewer projected hospitalisations under the same amount of social contacts. 2) It enables the communication of more fine-grained results to policymakers, for which we experienced a demand during the COVID-19 pandemic. Third, the spatially explicit model with finely-grained mobility data allows to assess the impact of interprovincial mobility in the early stages of an epidemic, which is not possible with the national model. We found this impact to be limited for SARS-CoV-2 in Belgium, but this may not necessarily be the case in larger, poorly connected countries or for other infectious diseases; it is possible and interesting to mobilise the presented model for such purposes, which is arguably its most valuable scientific contribution.

Supplementary information. This paper contains additional information on the geography of Belgium (Appendix A.1), details with regard to the data used in this work (Appendices A.1, A.2 and B), more details on the implementation of the VOCs, seasonality, and vaccines (Appendix C), an overview of the model parameters and assumptions (Appendix D) and more details with regard to the model calibration (Appendix E).

Author contributions. **Tijs W. Alleman:** Conceptualisation, Software, Methodology, Investigation, Data curation, Writing – original draft. **Michiel Rollier:** Conceptualisation, Methodology, Investigation, Data curation, Writing – original draft. Both of the above authors have closely collaborated on the manuscripts contents and should both be regarded as the primary authors of the text. **Jenna Vergeynst:** Conceptualisation, Investigation, Project administration. **Jan M. Baetens:** Conceptualisation, Funding acquisition, Project administration, Writing – review & editing.

Acknowledgements. The resources and services used in this work were provided by the VSC (Flemish Supercomputer Center), funded by the Research Foundation - Flanders (FWO) and the Flemish Government. We would like to thank Proximus for providing the the telecommunication data free-of-charge. We would like to thank Lander De Visscher for his methodological help on the *Markov-Chain Monte-Carlo* technique used in this work. This work was supported by the UGent Special Research Fund, Belgium, by the Research Foundation Flanders (FWO), Belgium, project numbers G0G2920 and 3G0G9820 and by VZW 100 km Dodentocht Kadee, Belgium through the organisation of the 2020 100 km COVID-Challenge.

Conflict of interest. None declared.

Ethics approval. All used data conform to GDPR standards.

Consent to participate. Not applicable

Consent for publication. All authors consent to publication in Applied Mathematics and Computation, preceded by pre-print publication in an open-access archive.

Availability of data and materials. The COVID-19 hospitalisation data [43], seroprevalence data [42, 43], Google Community Mobility data [36] and the pre-pandemic contact matrices for Belgium [34] are publicly available. The telecommunication data to describe the mobility between the Belgian provinces is private.

Code availability. The source code for the presented models is freely available on GitHub in the public repository UGentBiomath/COVID19-Model. Reproducing the simulations of the spatially explicit COVID-19 model requires access to telecommunication data that is not publicly available. All data to run the nation-level COVID-19 model is readily available on GitHub.

Appendix A Data

A.1 COVID-19 time series data

The model parameters β^R , β^U , β^M , $\Omega^{\text{work, schools}}$, Ω^{rest} , M , $K_{\text{inf},\alpha\beta\gamma}$, $K_{\text{inf},\delta}$ and A are calibrated using the 11 provincial time series for daily new hospitalisations. The motivation to use these data are fourfold. First, as long as the total hospital capacity is not surpassed, which has not happened in Belgium, the number of hospitalisations is a more objective measure than the daily number of newly detected cases. After all, the latter is highly dependent on the available test capacity. Second, pressure on hospitals is the most relevant measure when informing policy decisions. From a public health perspective, one primarily wants to avoid excess pressure on hospitals, which results in postponement of non-COVID-19 care and eventually the collapse of the health care system. Third, these time series are preferred over data for ICU admissions or deaths, because due to the low number of counts, these data are very noisy, especially at the provincial level. Fourth, the daily number of hospitalisations does not depend on hospital dynamics, such as residence times and distributions between wards.

The model calibration secondarily relies on seroprevalence data, indicating the rate at which antibodies wane and thus the rate at which humoral immunity is lost. The seroprevalence time series is the estimated percentage of the population with SARS-CoV-2 antibodies in the blood, reflecting how many subjects have recovered from COVID-19. Demonstrating the model's ability to match the seroprevalence in the Belgian population is an important gauge for overall model fidelity. In this way it is possible to demonstrate that the model captures the total number of asymptomatic infections. We assume that new VOCs and vaccines do not alter the seroreversion rate over the calibration period.

Sciensano hospitalisation data

Sciensano, the national public health institute of Belgium [43], gathers and processes COVID-19-related hospitalisation time series at the provincial level from all 104 Belgian hospitals. This data set is updated daily, is exhaustive since March 15th 2020, and is anonymous (aggregated over all ages). It contains the number of newly-admitted lab-confirmed COVID-19 hospital patients in the last 24 hours, not referred from another hospital. This number excludes the patients that were admitted to the hospital for other reasons but tested positive for COVID-19 in a screening context. Seven-day moving-average time series for daily new hospitalisations are shown per province in Fig. A1. Provinces are denoted according to their NIS code (Table A1).

The used hospitalisation time series are exhaustive and of high quality, but two limitations should be noted. First, there is a *weekend effect* in the raw time series. This is mainly due to fewer hospitals reporting data over the weekend

and does not reflect viral dynamics; the effect is hence not captured by the model. Second, patients are recorded in the province they are hospitalised, not their province of residence. Thus, a patient residing in province g but hospitalised in province h is counted as a data point in province h . Since there is no way to circumvent this problem without considerable privacy issues, we must assume that at the level of provinces this effect is negligible.

Seroprevalence data

We consider two independent nationally aggregated time series containing information on the extrapolated number of Belgians that have a significant amount of anti-SARS-CoV-2 antibodies in residual serum samples (i.e. seroprevalence) – See Fig. A3. The first time series was gathered by Herzog et al. [42] between March 30th and October 17th 2020, and contains 7 data points from 3500 samples per collection period, spread over both sexes, all ages and all provinces (see Table 1 in [42]). Residual serum samples in this study originated from ambulatory patients (including people living in nursing homes) visiting their doctor (mainly general practitioners) for any reason including primary care, routine check-up or follow-up of pathology. The second time series was gathered by Sciensano [43] between March 30th 2020 and July 20th 2021, and contains 29 data points from 1000 samples per collection period, again homogeneously spread throughout Belgium. The blood samples originate from Red Cross blood donors. Combining both data sets is therefore interesting, as it contains both subjects in need of medical attention and healthy subjects capable of donating blood. The larger time period over which the latter study is conducted, implies that the data start to show the prevalence of anti-SARS-CoV-2 antibodies resulting from vaccination. This, combined with the acquisition of natural immunity, causes the percentage of ‘immune’ subjects to approach 100% by the summer of 2021 (see Fig. A3).

A.2 Mobility time series data

Origin and nature of the data

Proximus is Belgium’s largest telecommunication company with a market share of 30-40% in terms of active SIM cards [47]. Based on the connection between a user’s SIM card and the closest transmission tower, the approximate position of a SIM card is known at all times at which the device is operational. The amount of time that this device spends connected to a particular transmission tower is registered, on the condition that it has *reconnected* to a transmission tower and stays connected to this tower for over 15 minutes. Reconnecting occurs either by switching on a disabled device, or by travelling around – either within or outside a particular postal code. For any given Belgian province, the number of tracked SIM cards represents 25-50% of the province’s population. The extrapolation factor is calculated on a daily basis, based on the number of devices used by individuals living in

a particular postal code, and the total registered population there.

No data is available for times indicated by the hatched periods in Fig. 4, so we estimate $P^{gh}(t)$ values at these times based on particular periods in the available data. For business days (resp. weekends) before February 10th 2020, we take the average $P^{gh}(t)$ values over all business days (resp. weekends) between February 10th and March 1st 2020. For business days (resp. weekends) after August 31st 2021, we take the average over all business days (resp. weekends) between July 1st and August 31st 2021 (the summer holiday).

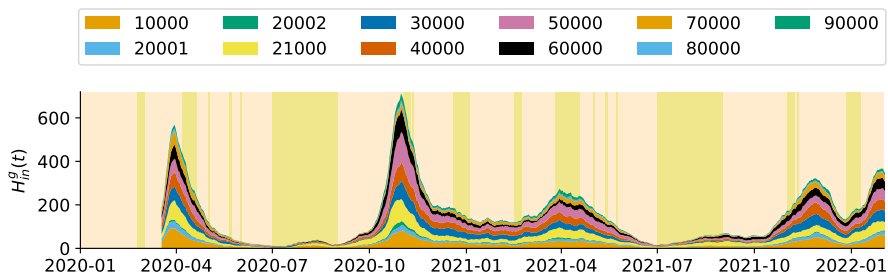


Fig. A1 Stacked area plot of all seven-day moving-averaged time series for daily new hospitalisations per province (denoted with NIS code, see Table A1) [43]. Daily data is available from March 15th 2020 onward.

Table A1 All 10 provinces and Brussel-Capital Region (the “11th province” for convenience). We denote the population density classification, the systematic name (NIS code), and which region it is in (Flanders, Brussels-Capital, Wallonia). We also denote their registered population and the number of hospitals that report the daily number of new COVID-19 patients.

Type	NIS	Name	Region	Population	# hospitals
Metropolitan	21000	Brussels	B	1 218 255	15
Urban	10000	Antwerpen	F	1 869 730	14
	20001	Vlaams-Brabant	F	1 155 843	6
	40000	Oost-Vlaanderen	F	1 525 255	14
Rural	20002	Brabant Wallon	W	406 019	2
	30000	West-Vlaanderen	F	1 200 945	11
	50000	Hainaut	W	1 346 840	14
	60000	Liège	W	1 109 800	12
	70000	Limburg	F	877 370	7
	80000	Luxembourg	W	286 752	3
	90000	Namur	W	495 832	6

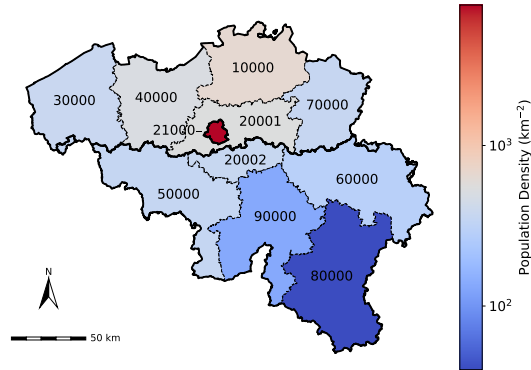


Fig. A2 Map of the Belgian provinces indicated by their NIS code (Table A1). The average population density is indicated by the colour scheme and determines whether we consider a province to be rural, urban or metropolitan, with threshold values resp. 400 km^{-2} and 4000 km^{-2} .

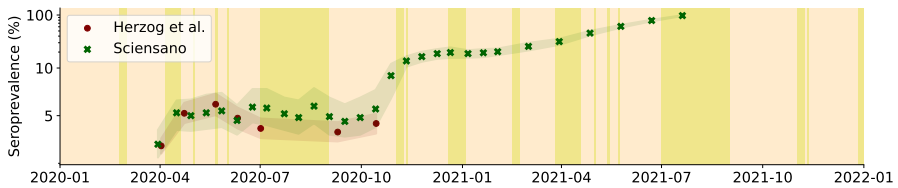


Fig. A3 Timeline with seroprevalence data from randomly sampling subjects visiting the general practitioner (Herzog et al. [42], maroon), or Red Cross blood donors (Sciensano [43], green). The data is space- and age-aggregated and expressed as a percentage of the total population. The band around the data shows the 95% uncertainty interval. Note the symmetrical log scale on the y axis.

Appendix B Social contact model

Scaling prepandemic contact matrices to model pandemic behaviour

The pandemic social behaviour of the Belgian population must be translated into a linear combination of prepandemic interaction matrices, given by

$$\mathbf{N}(t) = \text{span}(\mathbf{N}^{\text{home}}, \mathbf{N}^{\text{schools}}, \mathbf{N}^{\text{work}}, \mathbf{N}^{\text{transport}}, \mathbf{N}^{\text{leisure}}, \mathbf{N}^{\text{others}}). \quad (\text{B1})$$

These interaction matrices are available through contact studies for different places k , namely, at home, in schools, in workplaces, during leisure activities, on public transport and during *other* activities [34]. We have to find coefficients so that the linear combination of prepandemic interaction matrices (Eq. (B1)) is a good representation of macroscopic social behaviour throughout the pandemic. Ideally, pandemic contact matrices are used as these will better represent mixing behaviour under lockdown measures. However, such matrices were not available at the start of the pandemic and thus our model was built upon prepandemic knowledge of social behaviour to make a prediction on pandemic social behaviour. First, Google Community Mobility Reports (GCMR) indicators for Workplaces, Transit stations, Retail & recreation and Groceries & pharmacy are used as proxies to scale the work, transport, leisure and *other* social contact matrices.

Google Community Mobility Reports

Social contact is rescaled daily based on data publicly provided in the GCMR [36]. These data are available for (virtually) every day since February 15th 2020, and are expressed as fractions of “activity” compared to the median value from the 5-week period between January 3rd and February 6th, 2020. This activity is quantified as an anonymous aggregated GPS-informed visitation frequency to six location types (retail & recreation, grocery, parks, transport, work, and residential). We call these unprocessed time series the GCMR indicators, or mathematically, $\mathcal{G}(t)$ with elements $\mathcal{G}^{g,k'}(t)$ for every province g and every activity type k' . The time series $\mathbf{G}^k(t)$, used to rescale the prepandemic contact matrices \mathbf{N}^k , are derived from $\mathcal{G}(t)$ as follows:

$$\left\{ \begin{array}{l} \mathbf{G}^{\text{home}}(t) = 1, \\ \mathbf{G}^{\text{school}}(t) = \mathbf{H}(t), \\ \mathbf{G}^{\text{work}}(t) = \mathcal{G}^{\text{work}}(t), \\ \mathbf{G}^{\text{transport}}(t) = \mathcal{G}^{\text{transport}}(t), \\ \mathbf{G}^{\text{leisure}}(t) = \mathcal{G}^{\text{retail \& recreation}}(t), \\ \mathbf{G}^{\text{other}}(t) = \mathcal{G}^{\text{grocery}}(t). \end{array} \right. \quad (\text{B2})$$

The GCMR includes an indicator for residential mobility as well. During lockdowns, residential mobility increases and this is indicative of decreased community mobility. Although the mobility figures indicate people spend more time at home during lockdown (see Fig. 2 in [2]), this does not mean people have more contacts at home. Increasing the fraction of household contacts

under lockdown measures would increase intergenerational mixing of the population and this is not realistic or desired when modelling social restrictions. Hence, we assume home mobility remains the same throughout the entire pandemic and thus $G^{\text{home}}(t) = 1$. $\mathbf{H}(t)$ with elements $H^g(t)$ equals 1 when schools are open, and 0 otherwise. All $G^k(t)$ are assumed equal to 1 before the start of the dataset on February 15th 2020. The resulting time series $\mathbf{G}^k(t)$ are shown in Fig. B4.

Effectivity parameters

Intuitively, the effectivity of a contact in a given location may not scale linearly with the observed mobility reductions. The net effectivity of the contacts under lockdown depends on a combination of the prepandemic physical proximity and duration of the contact, the effectivity of preventive measures and on behavioural changes during lockdown. As an example, the effects of alcohol gel and face masks might be significant in workplaces and in grocery stores, but not at home or during leisure activities. To account for different effectivities of contacts in different places, we could introduce one additional parameter per location k , denoted Ω_k , but this would require inferring six additional parameters based on the hospitalisation, which would result in identifiability issues and thus simplifications must be made.

First, we found that the effectivity parameters of public transport and other places could not be identified. Likely because few contacts are made in these places [48]. Consequently, the effectivity parameters of public transport, other places and leisure contacts were aggregated, as such reducing the number of effectivity parameters from six to four. Second, as previously mentioned, the home contacts are not scaled with the residential GCMR indicator but rather it is assumed that $G^{\text{home}} = 1$. The analytic expression of the basic reproduction number of the (equivalent) national model is [2],

$$R_0 = \beta(ad_a + \omega)N,$$

where β is the per contact chance of SARS-CoV-2 transmission, a is the fraction of asymptomatic individuals, d_a the length of the asymptomatic infectious period, ω the length of the presymptomatic infectious period and N the total number of social contacts. A constant contribution of home contacts (constituent of N) is strongly correlated with the infectivity parameters in the model (β), which makes Ω_{home} (structurally) unidentifiable. We thus assume $\Omega_{\text{home}} = 1$. Third, when calibrating Ω_{schools} , Ω_{work} and Ω_{leisure} from March 15th, 2020 until October 14th, 2021, effectivities in schools close to zero are inferred. Because changes in school and work contacts often coincide, during holidays schools are closed and workplace mobility is lower, practical unidentifiability exists between the effectivities of contacts in schools and workplaces. So, we assume that $\Omega_{\text{schools}} = \Omega_{\text{work}} = \Omega_{\text{work, schools}}$. Al together, only two effectivity parameters, $\Omega_{\text{work, schools}}$ and Ω_{leisure} are inferred from the data.

Mentality parameter

During model development, we observed that the number of effective social contacts becomes smaller than the number of contacts obtained after rescaling with the GCMR indicators and the effectivity parameters when strict social measures are taken. Thus, one additional parameter was introduced to additionally downscale the number of social contacts when lockdown measures are taken. The so-called *mentality* parameter $\mathbf{M}(t)$, with entries $M^g(t)$ for province g , is introduced over a two-week period in the social contact model every time lockdown measures are taken. Once the lockdown measures are released, it is gradually released from the social contact model over a two month period using a ramp function. The entries $M^g(t)$ for province g of $\mathbf{M}(t)$ are almost always identical, except during a brief period during August 2020, when minor manual tweaks had to be made to prevent mistakes during the summer of 2020 from propagating into the second 2020 COVID-19 wave (see Fig. B5). Walloon provinces were given a mentality value of one, representing "lockdown free" mentality, while all Flemish provinces, except for West-Vlaanderen (NIS: 30000) were assigned the calibrated mentality value. During the model calibration procedure, the value of mentality aside from August 2020 was inferred as $M^g = 0.61 \pm 0.05$ for all provinces g . The introduction of the mentality parameter adds a degree of freedom to the model that can be re-estimated when social context changes in the future or when different measures are taken in different spatial patches of the model.

Pandemic contact model

After rescaling our prepandemic contact matrices with the GCMR indicators, and after introducing the effectivity (Ω_x) and mentality ($\mathbf{M}(t)$) parameters, the linear combination of prepandemic interaction matrices used to model pandemic social contact becomes,

$$\begin{aligned} \mathbf{N}(t) = \mathbf{N}^{\text{home}} + \mathbf{M}(t) \left\{ \Omega^{\text{work, schools}} \left[\mathbf{G}^{\text{schools}}(t) \mathbf{N}^{\text{schools}} + \mathbf{G}^{\text{work}}(t) \mathbf{N}^{\text{work}} \right] \right. \\ \left. + \Omega^{\text{rest}} \left[\mathbf{G}^{\text{transport}}(t) \mathbf{N}^{\text{transport}} + \mathbf{G}^{\text{leisure}}(t) \mathbf{N}^{\text{leisure}} + \mathbf{G}^{\text{other}}(t) \mathbf{N}^{\text{other}} \right] \right\}. \end{aligned} \quad (\text{B3})$$

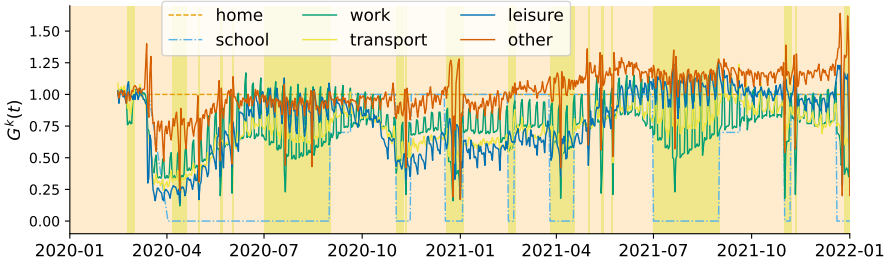


Fig. B4 Nationally averaged values of the GCMR indicators ($G^k(t)$) used for rescaling of the social contact matrices (Eq. (4)). The contact matrices for home and school contacts are not scaled with their respective GCMR indicator (motivated in [2]). The contact matrices for the other social environments (workplaces, transport, leisure and *other* places) are scaled with their appropriate GCMR indicator. The model uses such time series for every province.

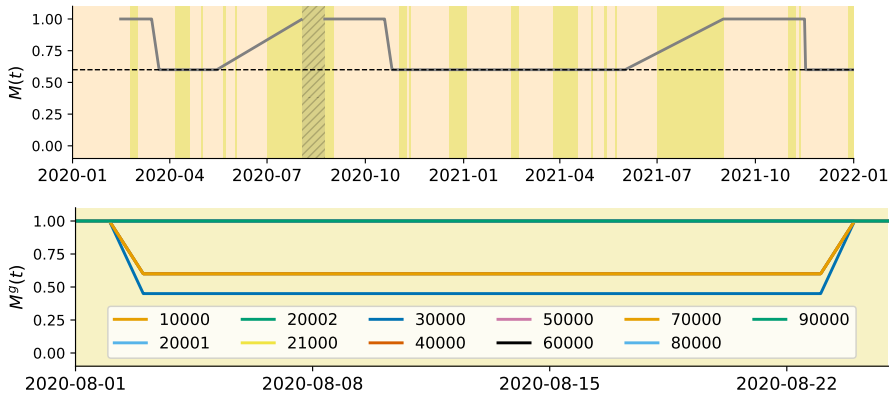


Fig. B5 *Top*: time-dependent mentality factor varying between the values of one and $M = 0.61 \pm 0.05$. Here, a value of one indicates people behave as if awareness for SARS-CoV-2 is low. The value of 61 % represents the additional contact multiplier observed during lockdowns due to raised awareness for SARS-CoV-2 and was obtained during model calibration. The hatched area represents the period in August 2020 where mentality parameters had to be manually set for different provinces.

Appendix C Variants of concern, vaccination, and seasonality

C.1 Variants of concern

VOCs are assumed to influence the model dynamics in three ways: 1) VOCs are associated with an increase of the transmission coefficients β compared to the wild-type variant, denoted K_{inf} , 2) VOCs can alter the hospital admission propensity of infected individuals compared to the wild-type variant, this is denoted as K_{hosp} , 3) VOCs are associated with different durations of the latent COVID-19 period σ . To account for 1) and 2) respectively, the infectivity parameters β^R , β^U and β^M are rescaled with the prevalence-weighted average infectivity increase at time t , and the hospital admission propensities (\mathbf{h}) are rescaled with the prevalence-weighted average hospital admission propensity gain at every time t . The relevant parameter values are listed in Table C2 and graphically illustrated in Fig. C6.

Table C2 VOC prevalence and VOC-dependent variables: infectivity increase of VOC type n compared to the wild type ($K_{\text{inf},n}$), hospitalisation propensity increase, and duration of the latent period. The values of $K_{\text{inf},n}$ were found during model calibration. Values of $K_{\text{hosp},n}$ and σ_n were extracted from [13–15, 40].

Parameter	wild type	α - β - γ	δ
$K_{\text{inf},n}$ (-)	1.00	1.28 \pm 0.09	1.61 \pm 0.11
$K_{\text{hosp},n}$ (-)	1.00	1.00	1.00
σ_n (days)	4.5	4.5	3.8

The VOC prevalence data (on the national level) were obtained from [39]. The increase in infectivity from the α - β - γ and δ VOCs compared to the wild-type were found during model calibration. The combination of the α - β - γ VOCs were estimated to be 28 \pm 9% more infectious than the wild-type, while the δ variant was estimated to be 61 \pm 11% more infectious than the wild-type. The combination of the α - β - γ VOCs almost certainly increased the hospital admission propensity. For instance, Grint et al. [13] reported an average increase of 62%. However, we found that applying such multipliers to the model’s hospitalisation propensity did not yield satisfactory results. Hence, for the sake of simplicity, we assume no increase of the hospitalisation propensity. The δ variant was shown to increase the hospital admission propensity for unvaccinated individuals with roughly 70% [14, 49]. On the other hand, a Norwegian study found no significant increase in hospital admission propensity [15].

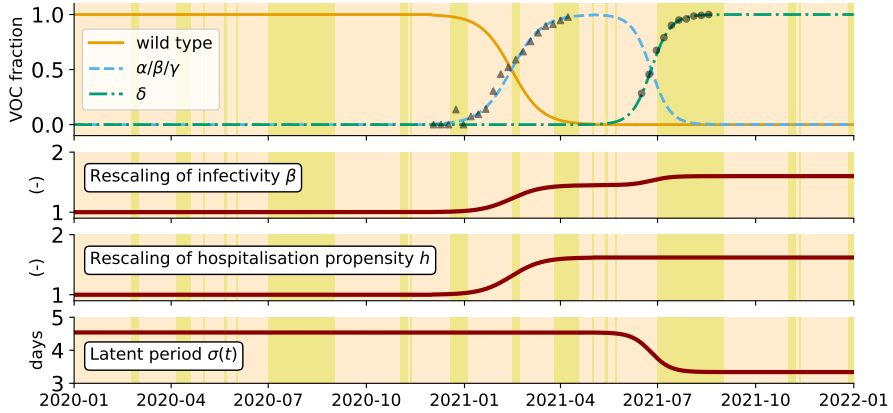


Fig. C6 *Top*: Prevalence of the wild-type variant, the α - β - γ variants (aggregated), and the δ variant in Belgium. Solid lines show a logistic fit in addition to raw data for α - β - γ (triangles) and δ (circles) [39, 41]. *Bottom*: Effect of the VOCs on resp. rescaling of the transmission coefficient $\beta(t)$, rescaling of the hospitalisation propensity $h(t)$, and time-dependent values of the latent disease period $\sigma(t)$ according to Eq. (6)) and values in Table C2.

C.2 Seasonality

The effect of seasonality on SARS-CoV-2 transmissibility is incorporated in a cosine function with a period of one year (Eq. (7), based on [21]). The introduction of seasonality rescales the transmissibility parameters β^R , β^U , β^M . Maximum transmissibility is assumed at January 1st and minimum transmissibility is assumed at July 1st. The amplitude of the cosine was estimated at $A_s = 0.19 \pm 0.04$ during model calibration. The seasonality influences viral transmission in ways considered out of this work's scope for this work, hence the simplicity of the seasonal relationship.

C.3 Vaccination

Our model uses vaccine incidence data to transfer individuals between the considered vaccination metapopulations (see Section 2.2). In every vaccine metapopulation, the vaccine offers protection through three mechanisms, each associated with its own efficacy and waning rate. By dynamically rescaling the efficacies of every vaccine metapopulation, the impact of vaccine waning is accounted for in a computationally inexpensive way (see Section 2.4).

Vaccine efficacies

Tartof et al. [18] demonstrated that, for an individual fully vaccinated with the mRNA-1273 (Pfizer) vaccine, protection against hospitalisation wanes slower than protection against symptoms. Similar findings were reported by Braeye et al. [50]. From an updated version of Braeye et al. [19] (informal communication), for every relevant VOC, the three vaccine efficacies of a partial vaccination (one dose), full vaccination (two doses) and boosted vaccination

(three doses) with mRNA-1273 could be extracted. In addition, the vaccine efficacies 200 days after a full vaccination (two doses) with mRNA-1273 could be extracted (Table C3). All vaccine efficacies are assumed equal to those of mRNA-1273 because 72% of vaccines administered by the end of the period considered during the model calibration (2021-10-01) were Pfizer's. We assume that partial vaccination offers half the protection a full vaccination offers, both 25 days and 175 days post-vaccination. No data was available on the waning of booster immunity at the time of writing, so we assumed the immunity of only partially and fully vaccinated individuals to wane. This assumption does not alter any of the results in this work. We assume that the vaccine efficacies for the wild-type variant are the same as the vaccine efficacies of the α - β - γ variant. This assumption has no impact on the results in this work because an appreciable amount of individuals had only been vaccinated when the α - β - γ variant became dominant.

Table C3 Efficacies of the vaccines in lowering the susceptibility to SARS-CoV-2, lowering the infectiousness of SARS-CoV-2, and the efficacies of the vaccines in lowering the hospitalisation propensity. Partial vaccination is assumed to result in half the efficacy of a full vaccination (both 25 days and 175 days post-vaccination). We assume that the vaccine efficacies for the wild-type variant are the same as the vaccine efficacies of the α - β - γ variant. Booster shots were not administered under the α - β - γ VOC. Protection against hospitalisation is retrieved for the δ VOC from Ref. [50] but assumed to same for the α - β - γ VOC. All $E_{\text{none},n}$ are 0.

	$E_{\text{partial},n}$	$E_{\text{full},n,0}$	$E_{\text{full},n,w}$	$E_{\text{booster},n,0}$
<i>Susceptibility</i>				
α - β - γ	0.44	0.87	0.64	NA
δ	0.40	0.79	0.54	0.80
<i>Infectiousness</i>				
α - β - γ	0.31	0.62	0.43	NA
δ	0.19	0.38	0.25	0.34
<i>Hospitalisation</i>				
α - β - γ	0.47	0.93	0.81	NA
δ	0.47	0.93	0.81	0.93

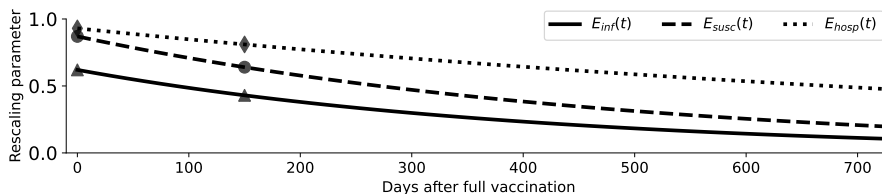


Fig. C7 Evolution of the vaccine efficacy associated with infectivity $E_{\text{inf}}(t)$, susceptibility $E_{\text{susc}}(t)$, and hospitalisation propensity $E_{\text{hosp}}(t)$ under the α - β - γ VOCs and over a two year period. The observations extracted from literature (see Table C3) were used to inform the half-life of the exponential decay function.

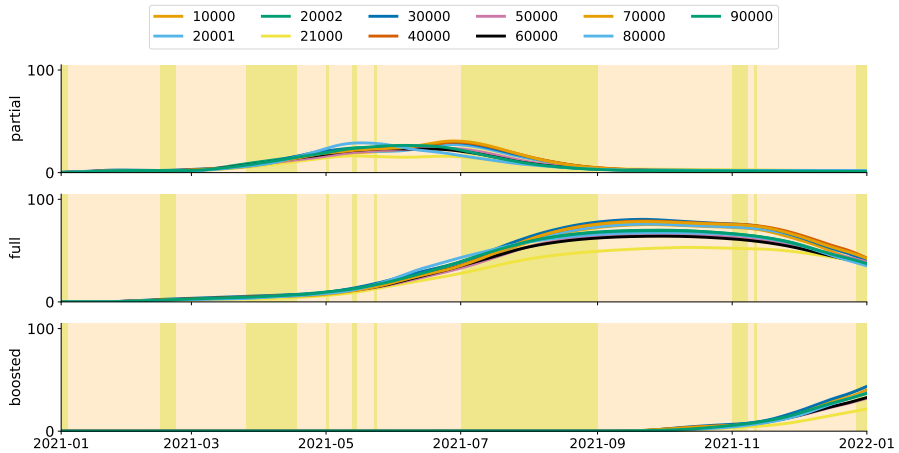


Fig. C8 Fraction of individuals in every province in the partially, fully and boosted vaccine metapopulations (indicated by NIS code, see Table A1). From top to bottom: first dose only (all vaccine types except Janssen), full dose only (second dose and Janssen vaccine), booster shot.

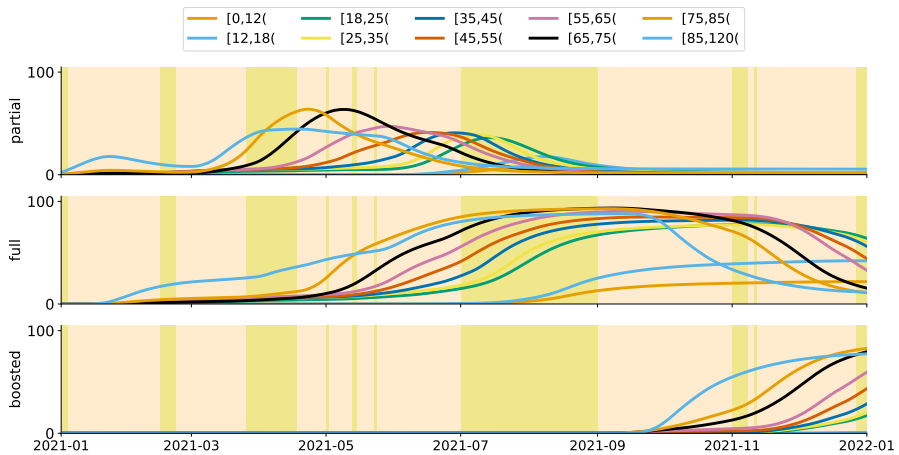


Fig. C9 Fraction of individuals in every age group in the partially, fully and boosted vaccine metapopulations. From top to bottom: first dose only (all vaccine types except Janssen), full dose only (second dose and Janssen vaccine), booster shot.

Appendix D Model parameters and assumptions

D.1 Model parameters

Table D4 Fraction of asymptomatic subjects a_i (based on [51]), and hospitalisation propensity h_i for symptomatic infections per age class (inferred, see [2]). The hospitalisation propensity \mathbf{h} is dynamically and spatially rescaled in the model to account for the combined effects of VOCs and vaccination. The baseline values without VOCs or vaccines are shown here.

Age class i (years)	a_i (%)	h_i (%)
[0, 12[81.9	1.0
[12, 18[81.9	1.0
[18, 25[78.8	1.5
[25, 35[77.6	2.5
[35, 45[73.6	3.0
[45, 55[69.5	6.0
[55, 65[67.1	12.0
[65, 75[64.5	40.0
[75, 85[51.1	70.0
[85, ∞ [35.4	99.0
Population average	71.4	14.7

Table D5 Average fraction c_i of hospitalised subjects admitted in a cohort ward (as opposed to an Intensive Care Unit), average mortality in cohort wards ($m_{C,i}$) and average mortality in ICU ($m_{ICU,i}$) per age class. These estimates were obtained by analysing a dataset of 22 136 patients in all 133 Belgian hospitals (see [2] for details).

Age class i (years)	c_i (%)	$m_{C,i}$ (%)	$m_{ICU,i}$ (%)
[0, 12[97.4	0.0	0.0
[12, 18[88.8	0.0	9.0
[18, 25[90.3	0.4	17.4
[25, 35[91.5	1.0	11.8
[35, 45[87.1	1.5	16.0
[45, 55[83.0	2.7	19.3
[55, 65[78.3	5.1	35.4
[65, 75[76.3	11.4	51.6
[75, 85[83.6	26.4	70.0
[85, ∞ [95.3	42.3	78.6
Population average	83.8	16.6	46.4

Table D6 Parameters used for calculating the dynamics between the various SEIQRD compartments shown in Fig. 2. Note that all symbols in boldface are non-scalar (vector or matrix), and the values of their elements are provided in separate tables.

Symbol	Parameter	Migration	Value
a	Fraction of infected subjects remaining asymptomatic	$I_{\text{presy}} \rightarrow I_{\text{asy}}$	Table D4, [51]
$h(t)$	Fraction of mildly symptomatic subjects requiring hospitalisation. Time-dependent due to VOCs and vaccination.	$I_{\text{presy}} \rightarrow Q_{\text{mild, H}}$ or $Q_{\text{mild, R}}$	Table D4, <i>inferred</i>
c	Fraction of hospitalisations admitted in regular cohort hospital ward	$Q_{\text{mild, H}} \rightarrow Q_{\text{hosp}}$ or Q_{ICU}	Table D5, [2]
m_C	Mortality of patients in a cohort hospital ward	$Q_{\text{hosp}} \rightarrow D$	Table D5, [2]
m_{ICU}	Mortality of patients in an IC unit	$Q_{\text{ICU}} \rightarrow D$	Table D5, [2]
$d_{C,R}$	Length-of-stay in hospital cohort ward (outcome: recovered)	$Q_{\text{hosp}} \rightarrow R$	Table D8, [2]
$d_{C,D}$	Length-of-stay in hospital cohort ward (outcome: deceased)	$Q_{\text{hosp}} \rightarrow D$	Table D8, [2]
$d_{\text{ICU},R}$	Length-of-stay in an IC unit (outcome: recovered)	$Q_{\text{ICU}} \rightarrow Q_{\text{ICU, rec}}$	Table D8, [2]
$d_{\text{ICU},D}$	Length-of-stay in an IC unit (outcome: deceased)	$Q_{\text{ICU}} \rightarrow D$	Table D8, [2]
$d_{\text{ICU,rec}}$	Average recovery stay in a cohort ward after ICU	$Q_{\text{ICU,rec}} \rightarrow R$	Table D8, [2]
$\sigma(t)$	Average duration of latent period. Time-dependent due to VOCs.	$E \rightarrow I_{\text{presy}}$	Table C2
d_a	Average duration of asymptomatic infection	$I_{\text{asy}} \rightarrow R$	5.0 d, <i>assumed</i>
d_m	Average duration of mild infection before recovery	$Q_{\text{mild, R}} \rightarrow R$	5.0 d, <i>assumed</i>
d_{hosp}	Average duration between symptom onset and hospitalisation	$Q_{\text{mild, H}} \rightarrow Q_C$ or Q_{ICU}	6.4 d, [2]
ω	Average duration of presymptomatic infectious period	$I_{\text{presy}} \rightarrow I_{\text{asy}}$ or $Q_{\text{mild, R}}, Q_{\text{mild, H}}$	0.7 d, [28, 52]
ζ	Average seroreversion rate	$R \rightarrow S$	$\ln(2)/365$ d ⁻¹ , <i>assumed</i>
$\tilde{N}_{ij}^g(t)$	Number of social contacts made by age group i with individuals of age group j in province g on day t . Time-dependent due to dynamic rescaling with GCMR indicators.	$S \rightarrow E$	see Appendix B
$\beta(t)$	Probability of infection upon contact with an infectious individual (if the infectee is 100% susceptible), elements β^g and three degrees of freedom $\beta^R, \beta^U, \beta^M$. Time-dependent due to seasonality, VOC prevalence, and vaccination.	$S \rightarrow E$	[0.021, 0.021, 0.024], <i>inferred</i>

Table D7 Parameters of modules making model parameters $\beta(t)$, $\tilde{N}(t)$, $h(t)$ time-dependent model parameters.

Symbol	Parameter	Alters	Value
Social contact			
$\Omega_{\text{work, schools}}$	Effectivity of social contacts in workplaces and school for the transmission of SARS-CoV-2	$\tilde{N}(t)$	0.49, <i>inferred</i>
Ω_{rest}	Effectivity of social contacts of leisure activities, on public transport and in <i>other</i> places for the transmission of SARS-CoV-2	$\tilde{N}(t)$	0.64, <i>inferred</i>
M	Mentality. Additional reduction of social contacts under lockdown on top of reductions indicated by the GCMRs. Arguably due to mentality changes.	$\tilde{N}(t)$	0.61, <i>inferred</i>
Variants of Concern			
K_{inf}	Infectivity gain of VOCs (α - β - γ , δ) as compared to wild type	$\beta(t)$	[28 %, 61%], <i>inferred</i>
K_{hosp}	Hospitalisation propensity gain due to VOCs as compared to wild type	$h(t)$	Table C2
Seasonality			
A	Amplitude of seasonality in the viral transmissibility of SARS-CoV-2	$\beta(t)$	19 %, <i>inferred</i>
Vaccination			
$E_{v, \text{susc}}(t)$	Efficacy of vaccine dose v in lowering susceptibility to SARS-CoV-2. Elements for every age group i and province g . Computed using vaccine incidence data and reported vaccine efficacies to obtain the average efficacy subject to waning.	$\beta(t)$	Dynamically scaled, see section C.3
$E_{v, \text{inf}}(t)$	Efficacy of vaccine dose v in lowering the infectiousness when infected with SARS-CoV-2. Elements for every age group i and province g . Computed using vaccine incidence data and reported vaccine efficacies to obtain the average efficacy subject to waning.	$\beta(t)$	Dynamically scaled, see section C.3
$E_{v, \text{hosp}}(t)$	Efficacy of vaccine dose v in lowering the hospitalisation propensity. Elements for every age group i and province g . Computed using vaccine incidence data and reported vaccine efficacies to obtain the average efficacy subject to waning.	$h(t)$	Dynamically scaled, see section C.3

Table D8 Hospital length-of-stay in a cohort ward (C) or intensive care unit (ICU) in case of recovery or death. NA denotes no deaths were recorded in that particular age class. These estimates were obtained by analysing a dataset of 22 136 patients in all 133 Belgian hospitals (see [2] for details).

Age class i (years)	$d_{C,R,i}$ (days)	$d_{C,D,i}$ (days)	$d_{ICU,R,i}$ (days)	$d_{ICU,D,i}$ (days)	$d_{ICU,rec,i}$ (days)
[0, 12[3.5	NA	5.9	NA	3.0
[12, 18[6.8	NA	3.2	16.0	4.0
[18, 25[5.7	2.0	5.3	3.0	4.0
[25, 35[4.8	8.1	9.3	12.6	4.5
[35, 45[5.9	6.0	10.9	16.3	5.0
[45, 55[6.9	8.8	11.4	20.6	6.0
[55, 65[8.5	8.7	12.7	17.3	6.0
[65, 75[11.2	13.2	13.8	16.3	8.0
[75, 85[15.2	12.1	11.9	13.6	11.0
[85, ∞ [18.9	11.8	5.0	9.1	10.0
Population average	10.8	11.8	12.0	15.2	5.6

D.2 Model assumptions and simplifications

Here, we list the assumptions and simplifications underpinning our model our model. While we consider these to not alter the paper’s conclusions, we choose to explicitly mention them below as good scientific practice.

1. Cross-border mobility is not included in this model, the mobility matrix, \mathbf{P} , is not age-stratified, and the elements $P^{gh}(t)$ were estimated when no data was available at time t (see Appendix A.2).
2. We assume that, on average, one only has work-related contacts in visited provinces, whereas all other types of contact are possible within the home province.
3. The GCMR indicators, which are used to inform the degree of social interaction in the model, are not age-stratified. The GCMR indicators thus present a more coarse-grained alternative to social-epidemiological contact studies under lockdown measures.
4. The average vaccine efficacies and information on vaccine waning used in the model were those of the Pfizer vaccine. The model does not explicitly distinguish between the different vaccines.
5. We aggregate the α , β and γ VOCs because the effect of their epidemiological properties are comparable in our model, and the aggregation decreases

A Stochastic Mobility-Driven Spatially Explicit SEIQRD COVID-19 Model with VOCs, Seas

the overall complexity.

6. Our model does not include age-specific increases for transmissibility and disease severity for the VOCs.
7. The emergence of the variants was implemented on the national level, thus, the geographic spread of the α - β - γ and δ variant was not included in the simulations.
8. We assume that new VOCs and vaccines do not alter the seroreversion rate.
9. Implementing seasonality using a cosine function is a high-level mathematical abstraction of several factors such as, but not limited to, the effects of humidity and temperature on viral survival in the environment.
10. In order for the negative binomial distribution log-likelihood function to apply to all $G \times n$ data points in the model calibration, the data points should strictly speaking be independent of each other, which they are not.
11. The model does not explicitly account for testing and tracing. These effects are implicitly accounted for in the calibrated parameters, however.
12. The model is based on ordinary differential equations (ODEs) and is thus deterministic in nature. This implies that epidemiological chain extinction is not possible and thus, at low SARS-CoV-2 prevalences, the model may overpredict the number of observed daily hospitalisations.
13. Raw vaccination data is only communicated for minors 0-17 years. There is no distinction for 0-12 or 12-17. In our current implementation, all vaccinations are distributed between 0-12 and 12-17 year olds based on demographics.
14. Vaccinated people are assumed to have the same number of contacts and the same mobility patterns as non-vaccinated people. Vaccinated people come into contact with the same fraction of vaccinated and non-vaccinated people as the national average, while some degree of segregation between vaccinated and non-vaccinated individuals could be expected.
15. The rate of transfer from the recovered to the susceptible pool, which influences the average duration of protection against reinfection does not depend on the vaccine stage.

Appendix E Model calibration

9 model parameters are considered to be a priori unknown and must be calibrated using the available data. Here we elaborate on the calibration procedure and the resulting parameter values and uncertainties.

E.1 Choosing an appropriate statistical model

Given a time series of daily hospitalisations \mathbf{x}^g for every province $g \in \{1, \dots, G\}$ with n observations x_t^g for $t \in \{1, \dots, n\}$ corresponding to times $\{t_1, \dots, t_n\}$, any choice for model parameters θ combined with an initial condition (IC) will produce a continuous time series $\tilde{x}^g(t)$ for every province g (after summing over all age groups and vaccination stages). This time series may be sampled to produce a set of model-based values $\{\tilde{x}^g(t_1), \dots, \tilde{x}^g(t_n)\}$ that we will denote as $\{\tilde{x}_1^g, \dots, \tilde{x}_n^g\}$. The aim is to find the model parameters for which it is most likely that the \mathbf{x}^g are observations of the modelled time series $\tilde{\mathbf{x}}^g$. An appropriate statistical distribution must be chosen to assess what deviations between \mathbf{x}^g and $\tilde{\mathbf{x}}^g$ are tolerable. To find the most appropriate statistical distribution, the relationship between the mean and variance of the time series \mathbf{x}^g must be studied. The time series for the daily number of hospitalisations consist of one observation per day without information on the variance. Mean-variance couples were *approximated* for all provincial time series using the following procedure,

1. Compute the (7-day) exponential moving average of the time series \mathbf{x}^g (solid red line in Figure E10). Assume it represents the *underlying truth*.
2. Subdivide the time series \mathbf{x}^g into discrete windows of length n days. Window lengths n of 7, 14 and 31 days were used with consistent results.
3. In every window, compute the mean observation and the variance between the exponential moving average and the observations.

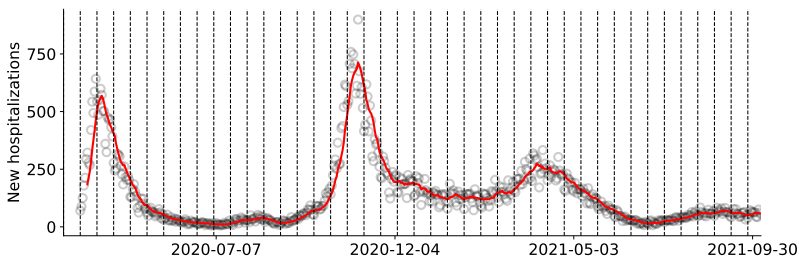


Fig. E10 National daily new hospitalisations (markers). Seven-day exponential moving average (solid red line).

Next, the most appropriate statistical model was chosen by fitting the mean-variance of several candidate distributions – the Gaussian model ($\sigma^2 =$

c), Poisson model ($\sigma^2 = \mu$), quasi-Poisson model ($\sigma^2 = \alpha\mu$) and negative binomial model ($\sigma^2 = \mu + \alpha\mu^2$) – and using the Akaike Information Criterion (AIC) to determine what model fits best. As an example, the result of the above analysis is shown for the national time series of daily hospitalisations in Figure E11. At the provincial level, the negative binomial model best described the variance in the data in all but two provinces, in which the quasi-Poisson model had the lowest AIC. However, for the sake of simplicity, it was assumed that all eleven provincial time series variance are described by the negative binomial model. In this way, we assume that a single observation x_t^g is the result of a counting experiment with an additional unknown error for every province g , captured by the estimated overdispersion parameter α^g per province g [44, 53] (see Table E9). The values of which were obtained by fitting the negative binomial mean-variance relationship to our estimated mean-variance couples. In general, the overdispersion in the data becomes larger when the population in a province decreases. The associated negative binomial likelihood for every observation t is

$$\mathcal{L}(\tilde{x}_t^g | x_t^g) = \frac{\Gamma(x_t^g + 1/\alpha^g)}{\Gamma(x_t^g + 1)\Gamma(1/\alpha^g)} \left(\frac{1/\alpha^g}{1/\alpha^g + \tilde{x}_t^g} \right)^{1/\alpha^g} \left(\frac{\tilde{x}_t^g}{1/\alpha^g + \tilde{x}_t^g} \right)^{x_t^g}, \quad (\text{E4})$$

with Γ the gamma function. The negative binomial distribution has mean value \tilde{x}_t^g and variance $\tilde{x}_t^g(1 + \alpha^g\tilde{x}_t^g)$; it is maximised for $\tilde{x}_t = x_t$ and reduces to the Poisson likelihood for $\alpha^g \rightarrow 0$. Adding more observations over time and regions, individual likelihood functions can be multiplied:

$$\mathcal{L}(\tilde{\mathbf{x}}|\mathbf{x}) = \prod_{g=1}^G \prod_{t=1}^n \mathcal{L}(\tilde{x}_t^g | x_t^g).$$

Again, this value $\mathcal{L}(\tilde{\mathbf{x}}|\mathbf{x})$ is maximised if $\forall g, t : \tilde{x}_t^g = x_t^g$, but this is generally not possible: the values \tilde{x}_t^g must be samples of the simulated local time series $\tilde{x}^g(t)$, for particular $\boldsymbol{\theta}$ values. Since the logarithmic function is monotonically increasing, the maximum value for $\mathcal{L}(\tilde{\mathbf{x}}|\mathbf{x})$ occurs at the same location in parameter space as for $\log \mathcal{L}(\tilde{\mathbf{x}}|\mathbf{x})$, so we may as well consider:

$$\begin{aligned} \log \mathcal{L}(\tilde{\mathbf{x}}|\mathbf{x}) = - \sum_{g=1}^G \sum_{t=1}^n \left(\log \left[\frac{\Gamma(x_t^g + 1/\alpha^g)}{\Gamma(x_t^g + 1)\Gamma(1/\alpha^g)} \right] + 1/\alpha^g \log \left[\frac{1/\alpha^g}{1/\alpha^g + \tilde{x}_t^g} \right] \right. \\ \left. + x_t^g \log \left[\frac{\tilde{x}_t^g}{1/\alpha^g + \tilde{x}_t^g} \right] \right). \end{aligned}$$

The result is the log-likelihood in Eq. (12). The parameter choice $\boldsymbol{\theta} = \hat{\boldsymbol{\theta}}$ that maximises Eq. (12) for the obtained values of α^g is considered the *best-fitting* choice. A large collection of such sampled $\hat{\boldsymbol{\theta}}$ make up the posterior. The posterior distributions resulting from the calibration MCMC also provide a quantitative measure for the calibrated value's uncertainty interval [54], which

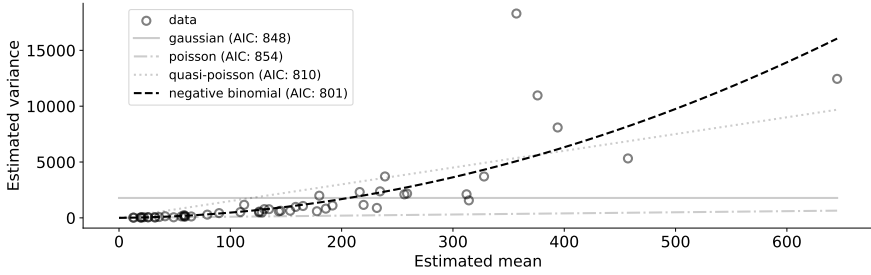


Fig. E11 Estimated mean-variance couples of the national time series of daily new hospitalisations, shown together with the fitted mean-variance models and their respective AIC scores.

together with the overdispersion values (α^g) determines the uncertainty on the simulated time series. Note that large \tilde{x}_t^g and x_t^g values will contribute more to the total sum in Eq. (12) than small such values, which means that time series of large provinces will have a larger weight in the overall sum. This effect is further amplified by the fact that less densely populated provinces generally have noisier data and thus larger overdispersion factors α^g . In our calibration procedure, we use three sources of data and thus, we optimise the weighted sum of three such log-likelihoods,

$$\log \mathcal{L}(\tilde{\mathbf{x}}_{H_{\text{in}}} | \mathbf{x}_{H_{\text{in}}}) + \log \mathcal{L}(\tilde{\mathbf{x}}_R | \mathbf{x}_{R, \text{Herzog}}) + \log \mathcal{L}(\tilde{\mathbf{x}}_R | \mathbf{x}_{R, \text{Sciensano}}),$$

The time series $\tilde{\mathbf{x}}_{H_{\text{in}}}$ and $\tilde{\mathbf{x}}_R$ correspond to the simulated daily new hospitalisations per province (summed over age groups and vaccine doses) and the total number of recovered subjects (summed over provinces, age groups, and vaccine doses), respectively. The observed time series are $\mathbf{x}_{H_{\text{in}}}$, $\mathbf{x}_{R, H}$ and $\mathbf{x}_{R, S}$: observed daily new hospitalisations per province [43], national seroprevalence data from general practitioners by Herzog et al. [42], and national seroprevalence data from Red Cross by Sciensano [43], respectively (see Appendix A.1).

Table E9 Values per province of the estimated overdispersion parameter of the negative binomial distribution associated with the time series of daily COVID-19 hospitalisations, used in the log-likelihood function (12). The average overdispersion coefficient of 0.034 (population-size weighted) was used for all simulations presented in this work.

Province	α^g	Province	α^g	Province	α^g
Antwerpen	0.031	West-Vlaanderen	0.041	Limburg	0.060
Vlaams-Brabant	0.035	Oost-Vlaanderen	0.027	Luxembourg	0.003
Brabant Wallon	0.059	Hainaut	0.029	Namur	0.007
Brussels	0.037	Liège	0.039		

E.2 Results of Model calibration

Calibrated values of all a priori unknown model parameters, including their interpretation, are listed in Table E10. The posterior distributions of the estimated parameters and their potential correlations are shown in Fig. E12. Simulations of the daily number of new hospitalisations for every province are shown in Figs E13 and E14. The small difference in goodness-of-fit between the spatially explicit and the national models is demonstrated in Fig. E15.

Table E10 All calibrated parameters in the spatially explicit SEIQRD model, with their physical interpretation and the equation that shows their mathematical definition. The values and confidence intervals of these parameters are determined in the MCMC procedure constructed around the log-likelihood function given by Eq. (12).

Param.	Interpretation	Eq.	Value	[$q_{0.025}$, $q_{0.975}$]
β^R	Transmission coefficient associated with rural provinces.	Eq. (5)	0.021	[0.019, 0.023]
β^U	Transmission coefficient associated with urban provinces.	Eq. (5)	0.021	[0.019, 0.023]
β^M	Transmission coefficient associated with metropolitan provinces.	Eq. (5)	0.024	[0.022, 0.027]
$\Omega^{\text{work, schools}}$	Effectivity parameter in work and school environments.	Eq. (2)	0.49	[0.37, 0.63]
Ω^{rest}	Effectivity parameter in transport, leisure and other environments.	Eq. (2)	0.64	[0.41, 0.84]
M	National mentality factor	Eq. (2)	0.61	[0.56, 0.65]
$K_{\text{inf}, \alpha\beta\gamma}$	Increased infectivity of the α - β - γ VOCs compared to the wild type for non-vaccinated subjects.	Eq. (6)	1.28	[1.21, 1.37]
$K_{\text{inf}, \delta}$	Increased infectivity of the δ VOC compared to the wild type for non-vaccinated subjects.	Eq. (6)	1.61	[1.51, 1.72]
A	Amplitude of seasonality in the viral transmissibility of SARS-CoV-2.	Eq. (7)	0.19	[0.15, 0.22]

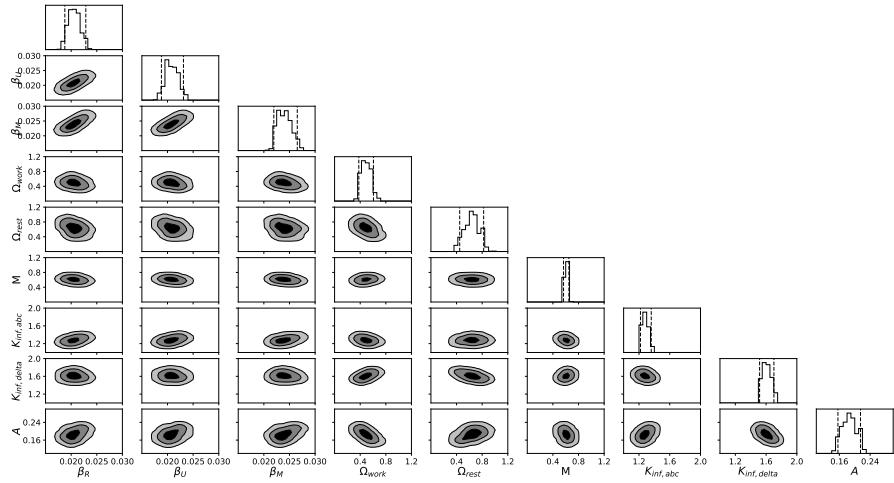


Fig. E12 Corner plot showing the posterior distributions of all 9 free parameters. Created with the `corner` package [55].

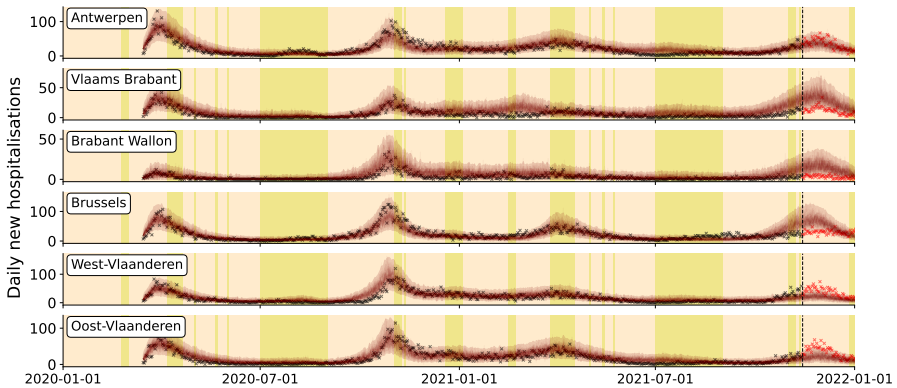


Fig. E13 100 model realisations of the daily new hospitalisations between March 15th 2020 and January 1st 2022 (solid lines) with a negative binomial 95% confidence region (transparent band). Black crosses signify raw data from Sciensano [43] were used in the calibration procedure while red crosses signify data were not used during the calibration procedure. From top to bottom: Antwerpen (10000), Vlaams Brabant (20001), Brabant Wallon (20002), Brussels (21000), West-Vlaanderen (30000) and Oost-Vlaanderen (40000). (see Table A1 and Fig. A2).

A Stochastic Mobility-Driven Spatially Explicit SEIQRD COVID-19 Model with VOCs, Seas

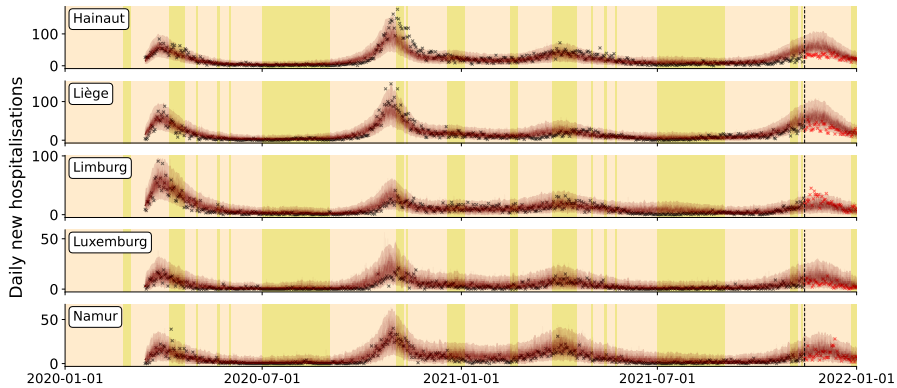


Fig. E14 100 model realisations of the daily new hospitalisations between March 15th 2020 and January 1st 2022 (solid lines) with a negative binomial 95% confidence region (transparent band). Black crosses signify raw data from Sciensano [43] were used in the calibration procedure while red crosses signify data were not used during the calibration procedure. From top to bottom: Hainaut (50000), Liège (60000), Limburg (70000), Luxembourg (80000), Namur province (90000) (see Table A1 and Fig. A2).

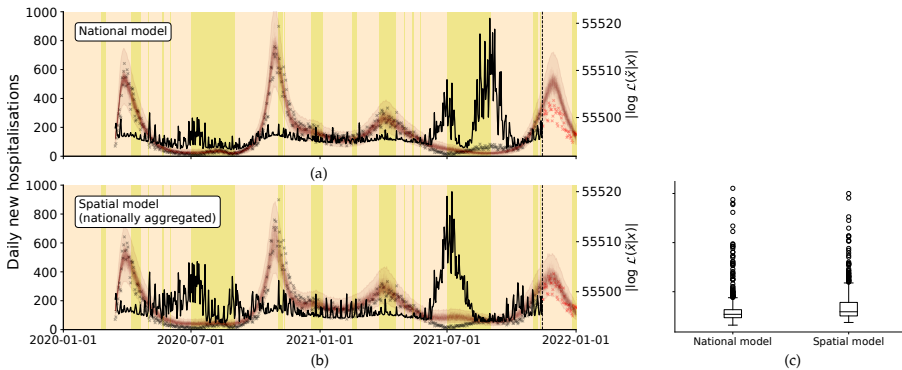


Fig. E15 (a) 100 realisations of the national model (see Ref. [2]) and (b) 100 realisations of the spatially explicit model (nationally aggregated) of the daily new hospitalisations between March 15th 2020 and January 1st 2022 (solid lines) with a negative binomial 95% confidence region (transparent band). The accompanying negative binomial log-likelihood score of the model predictions is given in black on the right hand axis. (c) Boxplot of the log-likelihood values at every time t of the national and spatially explicit model. Despite morphological differences, the goodness of fit of both models behaves in a similar manner: when SARS-CoV-2 prevalence is low, both models have difficulties being accurate.

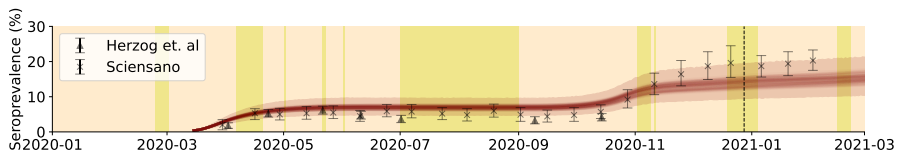


Fig. E16 (a) 100 realisations of the model estimated fraction of seropositive individuals (solid lines) with negative binomial 95% confidence region (transparent band) versus the fraction of seropositive individuals as measured by Refs. [42] and [43]. The dashed vertical line indicates the start of the nation-wide vaccination campaign (2020-12-28).

References

- [1] Zhu, N., Zhang, D., Wang, W., Li, X., Yang, B., Song, J., Zhao, X., Huang, B., Shi, W., Lu, R., Niu, P., Zhan, F., Ma, X., Wang, D., Xu, W., Wu, G., Gao, G.F., Tan, W.: A Novel Coronavirus from Patients with Pneumonia in China, 2019. *New England Journal of Medicine* **382**(8), 727–733 (2020). <https://doi.org/10.1056/nejmoa2001017>
- [2] Alleman, T.W., Vergeynst, J., De Visscher, L., Rollier, M., Torfs, E., Nopens, I., Baetens, J.M.: Assessing the effects of non-pharmaceutical interventions on sars-cov-2 transmission in belgium by means of an extended seiqrd model and public mobility data. *Epidemics* **37**, 100505 (2021). <https://doi.org/10.1016/j.epidem.2021.100505>
- [3] Abrams, S., Baetens, J.M., Vergeynst, J., Alleman, T.W., Nopens, I., Barbé, K., Vermolen, F., Franco, N., Clesse, S., Willem, L., Faes, C., Molenberghs, G., Beutels, P., Hens, N.: RESTORE Report 8: Long-term scenarios for the number of new hospitalizations during the Belgian COVID-19 epidemic. *ResearchGate* (2021). <https://doi.org/10.13140/RG.2.2.31704.83208>
- [4] Alleman, T.W., Rollier, M., Baetens, J.: Effect of Non-pharmaceutical Interventions on the Number of New Hospitalizations During the Fall 2021 Belgian COVID-19 Wave - Version 1.1. Report available on ResearchGate. https://www.researchgate.net/publication/356289190_Effect_of_non-pharmaceutical_interventions_on_the_number_of_new_hospitalizations_during_the_fall_2021_Belgian_COVID-19_wave_-_version_11
- [5] Alleman, T.W., Rollier, M., Baetens, J.: Effect of Non-pharmaceutical Interventions on the Number of New Hospitalizations During the Fall 2021 Belgian COVID-19 Wave - Version 1.2. Report available on ResearchGate. https://www.researchgate.net/publication/356897839_Effect_of_non-pharmaceutical_interventions_on_the_number_of_new_hospitalizations_during_the_fall_2021_Belgian_COVID-19_wave_-_version_12
- [6] Rollier, M., Miranda, G., Vergeynst, J., Meys, J., Alleman, T., Van De Vijver, E., Surveillance, t.B.C.G.o.C.-H., Nopens, I., Baetens, J.: Mobility and the spatial spread of SARS-CoV-2 in Belgium. *arXiv* (2022). <https://doi.org/10.48550/ARXIV.2202.11528>
- [7] Iacus, S.M., Santamaria, C., Sermi, F., Spyrtatos, S., Tarchi, D., Vespe, M.: How human mobility explains the initial spread of covid-19. *JRC Technical Reports* (2020). <https://doi.org/10.2760/61847>

- [8] Barker, P., Hartley, D., Beck, A.F., Oliver, G.H., Sampath, B., Roderick, T., Miff, S.: Rethinking Herd Immunity: Managing the Covid-19 Pandemic in a Dynamic Biological and Behavioral Environment. *NEJM Catalyst* (2021). <https://doi.org/10.1056/CAT.21.0288>
- [9] Aschwanden, C.: Five reasons why COVID herd immunity is probably impossible. *Nature* **591**(7851), 520–522 (2021). <https://doi.org/10.1038/D41586-021-00728-2>
- [10] Arenas, A., Cota, W., Gómez-Gardeñes, J., Gómez, S., Granell, C., Matamalas, J.T., Soriano, D., Steinegger, B.: A mathematical model for the spatiotemporal epidemic spreading of covid19. medRxiv (2020) <https://arxiv.org/abs/https://www.medrxiv.org/content/early/2020/03/23/2020.03.21.20040022.full.pdf>. <https://doi.org/10.1101/2020.03.21.20040022>
- [11] Costa, G.S., Cota, W., Ferreira, S.C.: Metapopulation modeling of COVID-19 advancing into the countryside: an analysis of mitigation strategies for Brazil. medRxiv, 2020–050620093492 (2020). <https://doi.org/10.1101/2020.05.06.20093492>
- [12] Roques, L., Bonnefon, O., Baudrot, V., Soubeyrand, S., Berestycki, H.: A parsimonious approach for spatial transmission and heterogeneity in the COVID-19 propagation: Modelling the COVID-19 propagation. *Royal Society Open Science* **7**(12), 1–19 (2020). <https://doi.org/10.1098/rsos.201382>
- [13] Grint, D.J., Wing, K., Houlihan, C., Gibbs, H.P., Evans, S.J.W., Williamson, E., McDonald, H.I., Bhaskaran, K., Evans, D., Walker, A.J., Hickman, G., Nightingale, E., Schultze, A., Rentsch, C.T., Bates, C., Cockburn, J., Curtis, H.J., Morton, C.E., Bacon, S., Davy, S., Wong, A.Y.S., Mehrkar, A., Tomlinson, L., Douglas, I.J., Mathur, R., MacKenna, B., Ingelsby, P., Croker, R., Parry, J., Hester, F., Harper, S., DeVito, N.J., Hulme, W., Tazare, J., Smeeth, L., Goldacre, B., Eggo, R.M.: Severity of Severe Acute Respiratory System Coronavirus 2 (SARS-CoV-2) Alpha Variant (B.1.1.7) in England. *Clinical Infectious Diseases* (2021) <https://arxiv.org/abs/https://academic.oup.com/cid/advance-article-pdf/doi/10.1093/cid/ciab754/40836348/ciab754.pdf>. <https://doi.org/10.1093/cid/ciab754>. ciab754
- [14] Bager, P., Wohlfahrt, J., Rasmussen, M., Albertsen, M., Krause, T.G.: Hospitalisation associated with sars-cov-2 delta variant in denmark. *The Lancet Infectious Diseases* **21**(10), 1351 (2021). [https://doi.org/10.1016/S1473-3099\(21\)00580-6](https://doi.org/10.1016/S1473-3099(21)00580-6)
- [15] Veneti, L., Valcarcel Salamanca, B., Seppälä, E., Starrfelt, J., Storm, M.L., Bragstad, K., Hungnes, O., Bøås, H., Kvåle, R., Vold, L., Nygård,

- K., Buanes, E.A., Whittaker, R.: No difference in risk of hospitalization between reported cases of the sars-cov-2 delta variant and alpha variant in norway. *International Journal of Infectious Diseases* **115**, 178–184 (2022). <https://doi.org/10.1016/j.ijid.2021.12.321>
- [16] Abrams, S., Baetens, J.M., Vergeynst, J., Alleman, T.W., Nopens, I., Barbé, K., Vermolen, F., Franco, N., Clesse, S., Willem, L., Faes, C., Molenberghs, G., Beutels, P., Hens, N.: RESTORE Report 7: Long-term scenarios for the number of new hospitalizations during the Belgian COVID-19 epidemic (2021). https://covid-en-wetenschap.github.io/assets/restore/report_v7.0.pdf Accessed 2022-03-23
- [17] Polack, F.P., Thomas, S.J., Kitchin, N., Absalon, J., Gurtman, A., Lockhart, S., Perez, J.L., Pérez Marc, G., Moreira, E.D., Zerbini, C., Bailey, R., Swanson, K.A., Roychoudhury, S., Koury, K., Li, P., Kalina, W.V., Cooper, D., Frenck, R.W., Hammitt, L.L., Türeci, O., Nell, H., Schaefer, A., Ünal, S., Tresnan, D.B., Mather, S., Dormitzer, P.R., Sahin, U., Jansen, K.U., Gruber, W.C.: Safety and efficacy of the bnt162b2 mrna covid-19 vaccine. *New England Journal of Medicine* **383**(27), 2603–2615 (2020) <https://arxiv.org/abs/https://doi.org/10.1056/NEJMoa2034577>. <https://doi.org/10.1056/NEJMoa2034577>. PMID: 33301246
- [18] Tartof, S.Y., Slezak, J.M., Fischer, H., Hong, V., Ackerson, B.K., Ranasinghe, O.N., Frankland, T.B., Ogun, O.A., Zamparo, J.M., Gray, S., Valluri, S.R., Pan, K., Angulo, F.J., Jodar, L., McLaughlin, J.M.: Effectiveness of mrna bnt162b2 covid-19 vaccine up to 6 months in a large integrated health system in the usa: a retrospective cohort study. *The Lancet* **398**(10309), 1407–1416 (2021). [https://doi.org/10.1016/S0140-6736\(21\)02183-8](https://doi.org/10.1016/S0140-6736(21)02183-8)
- [19] Braeye, T., Catteau, L., Brondeel, R., van Loenhout, J., Proesmans, K., Cornelissen, L., Van Oyen, H., Stouten, V., Hubin, P., Billuart, M., Djiena, A., Mahieu, R., Hammami, N., Van Cauteren, D., Wyndham-Thomas, C.: Vaccine Effectiveness Against COVID19-Infection and Onward Transmission by Variant of Concern and Time Since Vaccination, Belgian Contact Tracing, 2021. *SSRN Electronic Journal* (2022). <https://doi.org/10.2139/SSRN.4000559>
- [20] Martinez, M.E.: The calendar of epidemics: Seasonal cycles of infectious diseases. *PLOS Pathogens* **14**(11), 1–15 (2018). <https://doi.org/10.1371/journal.ppat.1007327>
- [21] Liu, X., Huang, J., Li, C., Zhao, Y., Wang, D., Huang, Z., Yang, K.: The role of seasonality in the spread of covid-19 pandemic. *Environmental research* **195**, 110874–110874 (2021). <https://doi.org/10.1016/j.envres.2021.110874>. 33610582[pmid]

- [22] Daley, D.J., Gani, J.: Epidemic Modelling: An Introduction. Cambridge Studies in Mathematical Biology. Cambridge University Press, Cambridge (1999). <https://doi.org/10.1017/CBO9780511608834>
- [23] Gillespie, D.T.: Exact stochastic simulation of coupled chemical reactions. *The Journal of Physical Chemistry* **81**(25), 2340–2361 (1977). <https://doi.org/10.1021/j100540a008>
- [24] Gillespie, D.T.: Approximate accelerated stochastic simulation of chemically reacting systems. *The Journal of Chemical Physics* **115**(4), 1716–1733 (2001). <https://doi.org/10.1063/1.1378322>
- [25] Higham, D.J., Kloeden, P.E.: An Introduction to the Numerical Simulation of Stochastic Differential Equations, pp. 242–243. SIAM, Philadelphia (USA) (2021). Chap. 20
- [26] Kermack, W.O., McKendrick, A.G., Walker, G.T.: A contribution to the mathematical theory of epidemics. *Proceedings of the Royal Society of London. Series A, Containing Papers of a Mathematical and Physical Character* **115**(772), 700–721 (1927) <https://arxiv.org/abs/https://royalsocietypublishing.org/doi/pdf/10.1098/rspa.1927.0118>. <https://doi.org/10.1098/rspa.1927.0118>
- [27] Ganyani, T., Kremer, C., Chen, D., Torneri, A., Faes, C., Wallinga, J., Hens, N.: Estimating the generation interval for coronavirus disease (COVID-19) based on symptom onset data, March 2020. *Euro surveillance* **25**(17) (2020). <https://doi.org/10.2807/1560-7917.ES.2020.25.17.2000257>
- [28] Wei, W.E., Li, Z., Chiew, C.J., Yong, S.E., Toh, M.P., Lee, V.J.: Presymptomatic Transmission of SARS-CoV-2 — Singapore, January 23–March 16, 2020. *MMWR. Morbidity and Mortality Weekly Report* **69**(14), 411–415 (2020). <https://doi.org/10.15585/mmwr.mm6914e1>
- [29] Gudbjartsson, D.F., Helgason, A., Jonsson, H., Magnusson, O.T., Melsted, P., Norddahl, G.L., Saemundsdottir, J., Sigurdsson, A., Sulem, P., Agustsdottir, A.B., Eiriksdottir, B., Fridriksdottir, R., Gardarsdottir, E.E., Georgsson, G., Gretarsdottir, O.S., Gudmundsson, K.R., Gunnarsdottir, T.R., Gylfason, A., Holm, H., Jensson, B.O., Jonasdottir, A., Jonsson, F., Josefsdottir, K.S., Kristjansson, T., Magnusdottir, D.N., le Roux, L., Sigmundsdottir, G., Sveinbjornsson, G., Sveinsdottir, K.E., Sveinsdottir, M., Thorarensen, E.A., Thorbjornsson, B., Löve, A., Masson, G., Jonsdottir, I., Möller, A.D., Gudnason, T., Kristinsson, K.G., Thorsteinsdottir, U., Stefansson, K.: Spread of sars-cov-2 in the icelandic population. *New England Journal of Medicine* **382**(24), 2302–2315 (2020). <https://doi.org/10.1056/NEJMoa2006100>

- [30] Palchykov, V., Mitrović, M., Jo, H.-H., Saramäki, J., Pan, R.K.: Inferring human mobility using communication patterns. *Scientific Reports* **4**(1), 6174 (2014). <https://doi.org/10.1038/srep06174>
- [31] Ågren, K., Bjelkmar, P., Allison, E.: The use of anonymized and aggregated telecom mobility data by a public health agency during the covid-19 pandemic: Learnings from both the operator and agency perspective. *Data & Policy* **3** (2021). <https://doi.org/10.1017/dap.2021.11>
- [32] Santamaria, C., Sermi, F., Spyrtos, S., Iacus, S.M., Annunziato, A., Tarchi, D., Vespe, M.: Measuring the impact of covid-19 confinement measures on human mobility using mobile positioning data. a european regional analysis. *Safety Science* **132**, 104925 (2020). <https://doi.org/10.1016/j.ssci.2020.104925>
- [33] Kishore, N., Kiang, M.V., Engø-Monsen, K., Vembar, N., Schroeder, A., Balsari, S., Buckee, C.O.: Measuring mobility to monitor travel and physical distancing interventions: a common framework for mobile phone data analysis. *The Lancet Digital Health* **2**(11), 622–628 (2020). [https://doi.org/10.1016/S2589-7500\(20\)30193-X](https://doi.org/10.1016/S2589-7500(20)30193-X)
- [34] Willem, L., Hoang, T.V., Funk, S., Coletti, P., Beutels, P., Hens, N.: Socrates: An online tool leveraging a social contact data sharing initiative to assess mitigation strategies for covid-19. *medRxiv* (2020) <https://arxiv.org/abs/https://www.medrxiv.org/content/early/2020/03/19/2020.03.03.20030627.full.pdf>. <https://doi.org/10.1101/2020.03.03.20030627>
- [35] Hoang, T.V., Coletti, P., Kifle, Y.W., Kerckhove, K.V., Vercruyssen, S., Willem, L., Beutels, P., Hens, N.: Close contact infection dynamics over time: insights from a second large-scale social contact survey in Flanders, Belgium, in 2010-2011. *BMC Infectious Diseases* **21**(1), 1–15 (2021). <https://doi.org/10.1186/s12879-021-05949-4>
- [36] Google LLC: Google COVID-19 Community Mobility Reports (2020). <https://www.google.com/covid19/mobility/> Accessed 06-05-2020
- [37] Liu, H., Wei, P., Kappler, J.W., Marrack, P., Zhang, G.: Sars-cov-2 variants of concern and variants of interest receptor binding domain mutations and virus infectivity. *Frontiers in Immunology* **13** (2022). <https://doi.org/10.3389/fimmu.2022.825256>
- [38] Braeye, T., Cornelissen, L., Catteau, L., Haarhuis, F., Proesmans, K., De Ridder, K., Djiena, A., Mahieu, R., De Leeuw, F., Dreuw, A., Hammami, N., Quoilin, S., Van Oyen, H., Wyndham-Thomas, C., Van Cauteren, D.: Vaccine effectiveness against infection and onwards transmission of covid-19: Analysis of belgian contact tracing data, january-june 2021. *Vaccine*

- 39**(39), 5456–5460 (2021). <https://doi.org/10.1016/j.vaccine.2021.08.060>
- [39] Wenseleers, T.: Newcovid Belgium. GitHub (2021). https://github.com/tomwenseleers/newcovid_belgium
- [40] Hart, W.S., Miller, E., Andrews, N.J., Waight, P., Maini, P.K., Funk, S., Thompson, R.N.: Generation time of the alpha and delta sars-cov-2 variants: an epidemiological analysis. *The Lancet Infectious Diseases* (XXXX). [https://doi.org/10.1016/S1473-3099\(22\)00001-9](https://doi.org/10.1016/S1473-3099(22)00001-9)
- [41] Sciensano: Weekly Epidemiological Bulletin. Available at <https://covid-19.sciensano.be/sites/default/files/Covid19/Meest%20recente%20update.pdf> (2021). <https://covid-19.sciensano.be/sites/default/files/Covid19/Meest%20recente%20update.pdf>
- [42] Herzog, S., De Bie, J., Abrams, S., Wouters, I., Ekinici, E., Patteet, L., Coppens, A., De Spiegeleer, S., Beutels, P., Van Damme, P., Hens, N., Theeten, H.: Seroprevalence of igg antibodies against sars coronavirus 2 in belgium – a serial prospective cross-sectional nationwide study of residual samples (march – october 2020). medRxiv (2021) <https://arxiv.org/abs/https://www.medrxiv.org/content/early/2021/08/31/2020.06.08.20125179.full.pdf>. <https://doi.org/10.1101/2020.06.08.20125179>
- [43] Sciensano: EPISTAT. Available at <https://statbel.fgov.be/en/open-data/number-deaths-day-sex-district-age> (2020). <https://epistat.wiv-isp.be/covid/>
- [44] Chan, S., Chu, J., Zhang, Y., Nadarajah, S.: Count regression models for covid-19. *Physica A* **563**, 125460–125460 (2021). <https://doi.org/10.1016/j.physa.2020.125460>. 33162665[pmid]
- [45] Kennedy, J., Eberhart, R.: Particle swarm optimization. In: *Proceedings of ICNN'95 - International Conference on Neural Networks*, vol. 4, pp. 1942–19484 (1995). <https://doi.org/10.1109/ICNN.1995.488968>
- [46] Goodman, J., Weare, J.: Ensemble samplers with affine invariance. *Communications in Applied Mathematics and Computational Science* **5**(1), 65–80 (2010). <https://doi.org/10.2140/camcos.2010.5.65>
- [47] Federal Public Service Economy: Belgische telecommunicatie- en televisiesectoren (2019). <https://economie.fgov.be/nl/themas/online/telecommunicatie/belgische-telecommunicatie-en> Accessed 2021-05-18
- [48] Mossong, J., Hens, N., Jit, M., Beutels, P., Auranen, K., Mikolajczyk, R., Massari, M., Salmaso, S., Tomba, G.S., Wallinga, J., Heijne, J., Sadkowska-Todys, M., Rosinska, M., Edmunds, W.J.: Social contacts

- and mixing patterns relevant to the spread of infectious diseases. *PLoS Medicine* **5**(3), 0381–0391 (2008). <https://doi.org/10.1371/journal.pmed.0050074>
- [49] Twohig et al., K.A.: Hospital admission and emergency care attendance risk for sars-cov-2 delta (b.1.617.2) compared with alpha (b.1.1.7) variants of concern: a cohort study. *The Lancet Infectious Diseases* **22**(1), 35–42 (2022). [https://doi.org/10.1016/S1473-3099\(21\)00475-8](https://doi.org/10.1016/S1473-3099(21)00475-8)
- [50] Braeye, T., van Loenhout, J., Brondeel, R., Stouten, V., Hubin, P., Billuart, M., Chung, J., Vandromme, M., Wyndham-Thomas, C., Blot, K., Cateau, L.: Covid-19 vaccine effectiveness against symptomatic infection and hospitalization in belgium, july 2021-april 2022. *medRxiv* (2022). <https://doi.org/10.1101/2022.05.09.22274623>
- [51] Poletti, P., Tirani, M., Cereda, D., Trentini, F., Guzzetta, G., Sabatino, G., Marziano, V., Castrofino, A., Grosso, F., Del Castillo, G., Piccarreta, R., Andreassi, A., Melegaro, A., Gramegna, M., Ajelli, M., Merler, S., Force, A.L.C.-T.: Association of Age With Likelihood of Developing Symptoms and Critical Disease Among Close Contacts Exposed to Patients With Confirmed SARS-CoV-2 Infection in Italy. *JAMA Network Open* **4**(3), 211085–211085 (2021). <https://doi.org/10.1001/jamanetworkopen.2021.1085>
- [52] He, X., Lau, E.H.Y., Wu, P., Deng, X., Wang, J., Hao, X., Lau, Y.C., Wong, J.Y., Guan, Y., Tan, X., Mo, X., Chen, Y., Liao, B., Chen, W., Hu, F., Zhang, Q., Zhong, M., Wu, Y., Zhao, L., Zhang, F., Cowling, B.J., Li, F., Leung, G.M.: Temporal dynamics in viral shedding and transmissibility of COVID-19. *Nature Medicine* **26**(5), 672–675 (2020). <https://doi.org/10.1038/s41591-020-0869-5>
- [53] Cameron, A.C., Trivedi, P.K.: *Regression Analysis of Count Data* vol. *Econometric Society Monograph No.53*. Cambridge University Press, ??? (1998)
- [54] Foreman-Mackey, D., Hogg, D.W., Lang, D., Goodman, J.: emcee: The MCMC Hammer. *Publications of the Astronomical Society of the Pacific* **125**(925), 306 (2013) <https://arxiv.org/abs/1202.3665> [astro-ph.IM]. <https://doi.org/10.1086/670067>
- [55] Foreman-Mackey, D.: corner.py: Scatterplot matrices in python. *The Journal of Open Source Software* **1**(2), 24 (2016). <https://doi.org/10.21105/joss.00024>